Vision Research 158 (2019) 58–71

Contents lists available at ScienceDirect

Vision Research

journal homepage: www.elsevier.com/locate/visres

An alignment maximization method for the kinematics of the eye and eye-head fixations

Binbin Chen[a,*], Joanne Fielding[b,c], Hoam Chung[a]

[a] Department Mechanical and Aerospace Engineering, Monash University, Clayton, Victoria 3800, Australia
[b] School of Psychological Sciences, Monash Institute of Cognitive and Clinical Neurosciences, Monash University, Clayton, Victoria 3800, Australia
[c] Department of Neuroscience, Central Clinical School, Monash University, Melbourne, Victoria 3004, Australia

ARTICLE INFO

Number of Reviews = 2

Keywords:
Alignment
Donders' law
Listing's law
Vestibulo-ocular reflex
Head-free eye gaze
Eye-head coordination

ABSTRACT

The orientation of human eyes is uniquely defined with respect to their gaze direction, known as Donders' law. Further, the manner in which the eyes follow Donders' law varies as a function of the situation. When the head is stationary, the Donders' surfaces are flat planes but they tilt when eye fixation distance changes. These planes also shift and rotate when head orientation changes with respect to the direction of gravito-inertial acceleration. When the head is free to rotate, the Donders' surfaces are twisted. In this paper, we present a systematic method to analyze the kinematics of the eye under different gaze situations utilizing the measurement of alignment between various coordinate frames. Kinematic equations are presented for various eye movements ranging from simple head-fixed monocular shifts of eye gaze to complex eye-head shifts of gaze. At each stage, we show that simulated eye orientations that derived from our equations are able to capture the variations of Donders' surfaces and they are comparable with experimental results in the literature. The final equations we propose provide the unified kinematics of head-upright far gaze, head-upright binocular fixation, head static tilted monocular gaze and head-free monocular gaze.

1. Introduction

It is well known that both the eyes and the head are capable of rotating about three orthogonal axes in space, although three degrees of freedom (DOF) of movement are redundant for shifts of gaze as only two DOF are required to implement a change in gaze direction. Donders first discovered that the orientation of the human eye is not arbitrary but uniquely defined by the direction of gaze, regardless of how the eye reached that position (Donders et al., 1848; von Helmholtz & Southall, 2005). This is known as Donders' law. Donders' law couples the extra DOF, which constrains the three-dimensional eye orientations on a two-dimensional manifold. However, Donders' law does not specify the exact eye orientation for a given gaze direction.

Listing's law (L1) was later proposed for ocular orientation when the head is stationary and the two eyes are directed towards a distant target. L1 states that all orientations of the eye can be characterized by a single rotation from a reference position, and all rotation axes of the eye lie in a plane perpendicular to the reference position (Ferman, Collewijn, & Van den Berg, 1987; Tweed, Fetter, Andreadaki, Koenig, & Dichgans, 1992; Tweed & Vilis, 1990; von Helmholtz & Southall, 2005). This plane is called Listing's plane (LP) and the reference position is referred to as the primary position. L1 provides a quantitative account of Donders' law by numerically specifying the amount of torsion (Fetter, Haslwanter, Misslich, & Tweed, 1997).

Listing's law was initially proposed for distant vision. To accommodate near vision, L1 was later extended to include vergence. This is known as the binocular extension of Listing's law (L2). L2 states that, for near vision, vergence movements cause a temporal rotation of LP, where the amount of rotation is approximately one quarter of the eye vergence angle (Minken & Van Gisbergen, 1994; Mok, Ro, Cadera, Crawford, & Vilis, 1992; Van Run & Van den Berg, 1993; Wong, 2004). Similar to L1, L2 is only valid for eye fixations where the head is held immobile in an upright position.

The vestibulo-ocular reflex (VOR) is a compensatory eye movement that stabilizes the eye in space during translation and rotation of the head and body (Raphan & Cohen, 2002). The vestibular system in the inner ear detects angular and linear acceleration to generate a compensatory eye movement (Cohen & Raphan, 2004; Miller, 1962; Raphan & Cohen, 2002). The compensatory eye movement reduces retinal slip caused by head translation and rotation that lead to a violation of L1 (Angelaki, Zhou, & Wei, 2003; Crawford & Vilis, 1991; Misslisch & Hess, 2000).

* Corresponding author.
E-mail address: binbin.chen@monash.edu (B. Chen).

https://doi.org/10.1016/j.visres.2019.01.013
Received 24 July 2018; Received in revised form 12 December 2018; Accepted 5 January 2019
Available online 04 March 2019
0042-6989/

From a functional perspective, the VOR can be divided into two subsystems, the angular VOR (aVOR) and the linear VOR (lVOR) (Raphan & Cohen, 2002). The aVOR responds to the angular accelerations of head sensed by semicircular canals and the lVOR to the linear accelerations of head sensed by otolith organs. The static lVOR response refers to the lVOR response that is induced by stable linear accelerations. It has been observed that orientation of LP in the head changes with the orientation of the head relative to gravity (Bockisch & Haslwanter, 2001; Furman & Schor, 2003; Haslwanter, Straumann, Hess, & Henn, 1992; Misslisch, Tweed, & Hess, 2001; Nooij, Bos, & Groen, 2008). The position of LP shifts along the torsional axis by the static lVOR response when the head tilts to the side (roll tilt). The direction of the plane shift is opposite to that of the head roll (Bockisch & Haslwanter, 2001; Furman & Schor, 2003; Misslisch et al., 2001). When the head tilts forward or backward (pitch tilt), LP tilts in the opposite direction to the head (Furman & Schor, 2003; Haslwanter et al., 1992; Misslisch et al., 2001; Nooij et al., 2008).

When the head is free to rotate, eye-head coordination has both eye and head orientations following Donders' law (Glenn & Vilis, 1992; Radau, Tweed, & Vilis, 1994). The orientation of the eye in space and the orientation of the head in space in head-free eye gazes are similar to the orientations that are rotated by the Fick gimbal, where the Donders' surface plotted using the tip of the vector component of quaternions is twisted.

The existing research has focused on measuring eye and head movement in different situations to establish the functional significance of ocular torsion (Angelaki et al., 2003; Bockisch & Haslwanter, 2001; Clarke & Haslwanter, 2007; Crane, Tian, & Demer, 2006; Glenn & Vilis, 1992; Hess & Misslisch, 2016; Hess & Thomassen, 2014; Misslisch, Tweed, Fetter, Sievering, & Koenig, 1994; Misslisch et al., 2001; Mok et al., 1992; Nooij et al., 2008; Radau et al., 1994; Van Run & Van den Berg, 1993). However, a mathematical framework that can be extended to different types of eye and eye-head coordination utilizing the observed functions is rarely observed in the literature. Such a mathematical framework can provide a better understanding of control strategies behind the coordination of these functions.

As an attempt to establish a mathematical tool that is extendable from simple single eye movements to complicated eye-head coordination, we propose to utilize the measurement of alignments between various coordinate frames. We postulate that eye and the eye-head orientations maximize these measure of alignments. In order to validate the proposed approach, we first derive L1 by maximizing alignment between the frame fixed at the primary position and the frame fixed at the eye. We then demonstrate that this method can be extended to saccadic eye movement, vergence (L2), eye-head coordination in head-free gaze and static lVOR. Numerical simulations show that the eye orientations derived from the proposed method match well with experimental data in the literature.

This paper is organized as follows. In Section 2, we develop an alignment equation for simple head-fixed monocular eye gaze and show that eye orientations satisfy L1. The proposed method is used in head fixated saccades in Section 3. In Section 4, the head-fixed binocular eye fixations are investigated by using an additional alignment equation. Finally in Section 5, we extend the alignment equation developed in Section 2 to accommodate head movement, which is followed by conclusions and recommendations for future work.

2. Listing's Law in fixation

In distant vision, when the head is erect, L1 resolves the ambiguity of the redundant degree of freedom of the eye by constraining the rotation vector on LP. In the following, we show that L1 can be derived by maximizing alignment between the eye orientation and a "primary orientation".

We denote the primary orientation using a coordinate frame f_p. A

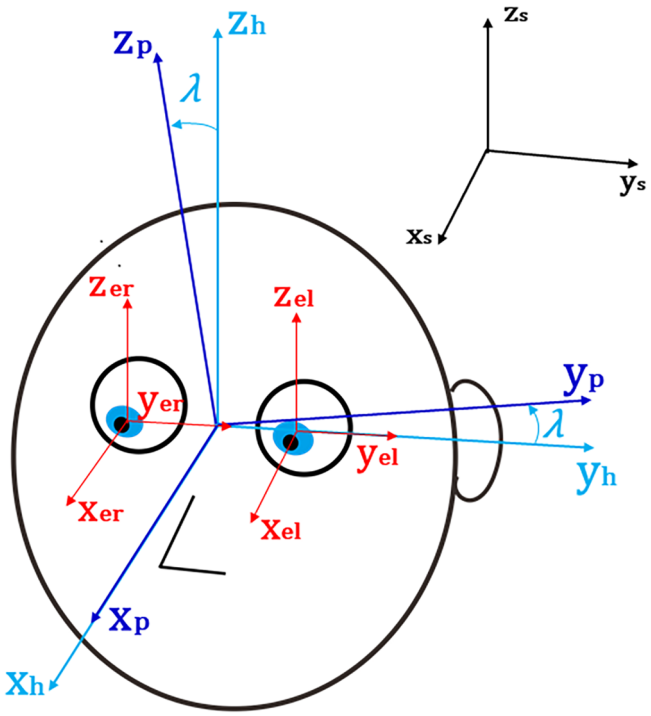

Fig. 1. Definition of coordinate frames.

coordinate frame f is composed of three orthonormal vectors $\mathbf{x}$, $\mathbf{y}$, and $\mathbf{z}$. Other than f_p, the coordinate frames f_s, f_h, f_{el}, and f_{er} are defined to represent the space, head, left eye, and right eye orientations respectively, as shown in Fig. 1. $\mathbf{F} \in \mathbb{R}^{3\times3}$ is defined to mathematically represent the orientation of f as

$$\mathbf{F} = [\mathbf{x} \quad \mathbf{y} \quad \mathbf{z}], \tag{1}$$

where $\mathbf{x}$, $\mathbf{y}$ and $\mathbf{z}$ are orthonormal vectors in $\mathbb{R}^3$.

The primary orientation f_p has $\mathbf{x}_p$ as the primary position in L1. Although the primary position varies between subjects and can deviate considerably from the eye center (Fetter et al., 1997; Tweed & Vilis, 1990), the primary position is assumed to be the forward straight gaze direction in this paper for simplicity. f_p is attached to the head (it rotates with the head) and only its orientation is of our interest. The location of f_p is not important and the same applies to all the other coordinate frames. The head frame f_h is located at the center of the head. $\mathbf{x}_h$ is towards to the naso-occipital direction, the same direction as $\mathbf{x}_p$. $\mathbf{y}_h$, and $\mathbf{z}_h$ are towards to the interocular direction and the head vertical direction, respectively. f_p and f_h are not necessary to have the same orientation and an angle λ is introduced to represent the angle of f_p tilted from f_h about their x axes. The spatial reference frame f_s is used to describes the spatial orientation sensed by the subject. $\mathbf{z}_s$ is pointing to the direction of Gravito-inertial Acceleration (GIA). However, $\mathbf{y}_s$ is depending on the body orientation. $\mathbf{y}_s$ is defined so that it is orthogonal to $\mathbf{z}_s$ and parallel with the body frontal plane. $\mathbf{x}_{el}$, $\mathbf{y}_{el}$, $\mathbf{z}_{el}$ and $\mathbf{x}_{er}$, $\mathbf{y}_{er}$, $\mathbf{z}_{er}$ are the orthogonal unit vectors of left eye frame f_{el} and right eye frame f_{er}, respectively. f_{el} and f_{er} are located at the center of the each eye and attached to the corresponding eyes. $\mathbf{x}_{el}$ and $\mathbf{x}_{er}$ are unit gaze vectors of the eyes.

Listing's law is about monocular eye orientation for distant vision and we use f_e instead of f_{el} or f_{er} in monocular vision. The alignment of f_e and f_p can be written as

$$A_{ep} = {}^{h}\mathbf{y}_e \cdot {}^{h}\mathbf{y}_p + {}^{h}\mathbf{z}_e \cdot {}^{h}\mathbf{z}_p. \tag{2}$$

The left superscript specifies the measurement frame of the vector. For example, ${}^{h}\mathbf{z}_p = [0 \quad -S_\lambda \quad C_\lambda]^T$ but ${}^{p}\mathbf{z}_p = [0 \quad 0 \quad 1]^T$. S_λ, C_λ and T_λ are the abbreviations of $\sin\lambda$, $\cos\lambda$ and $\tan\lambda$, which will be used throughout

the paper. Vector arithmetics can only be implemented between the vectors under the same measurement frame. All vectors in (2) are measured in the head frame. The dot product between ${}^{h}\mathbf{y}_e$ and ${}^{h}\mathbf{y}_p$ represents the alignment between the eye horizontal axis and the primary horizontal axis. The dot product between ${}^{h}\mathbf{z}_e$ and ${}^{h}\mathbf{z}_p$ represents the alignment between the eye vertical axis and the primary vertical axis. Therefore A_{ep} represents the total alignment between f_e and f_p. Note that, as long as two vectors are represented in a same frame, the result of dot product is independent of the choice of the measurement frame.

The orientation of a rigid body after rotations depends on the order of the rotations. This is a mathematical feature of rotational motions known as noncommutativity (Ghasia & Angelaki, 2005). There exist many evidences in the literature that the commutativity of rotations achieved by L1 is not likely to be a result of neural control (Ghasia & Angelaki, 2005; Miller, 2007) but a consequence of motor output (Demer, Oh, & Poukens, 2000; Kono, Clark, & Demer, 2002). We postulate that the minimum eye muscle stretch may be achieved by maximizing the alignment A_{ep} in Eq. (2), which is the mechanical property related to resolving the noncommutativity of eye rotations. In the following, we will show that by maximizing A_{ep}, the eye will follow L1. Suppose that the eye starts its movement at the primary position. In order for f_e to have the maximum alignment with f_p, the two frames must have the same orientation. Therefore, initial eye orientation will be ${}^{h}\mathbf{x}_{e0} = [1 \;\; 0 \;\; 0]^T$, ${}^{h}\mathbf{y}_{e0} = [0 \;\; C_\lambda \;\; S_\lambda]^T$, and ${}^{h}\mathbf{z}_{e0} = [0 \;\; -S_\lambda \;\; C_\lambda]^T$.

The following three rotation matrices are used to represent the three-dimensional rotations of f_e with respect to the head frame.

$$
\begin{aligned}
{}^{h}_{e}\mathbf{R}_z &= \begin{bmatrix} C_{\alpha_{\text{eh}}} & -S_{\alpha_{\text{eh}}} & 0 \\ S_{\alpha_{\text{eh}}} & C_{\alpha_{\text{eh}}} & 0 \\ 0 & 0 & 1 \end{bmatrix} \\
{}^{h}_{e}\mathbf{R}_y &= \begin{bmatrix} C_{\beta_{\text{eh}}} & 0 & S_{\beta_{\text{eh}}} \\ 0 & 1 & 0 \\ -S_{\beta_{\text{eh}}} & 0 & C_{\beta_{\text{eh}}} \end{bmatrix} \\
{}^{h}_{e}\mathbf{R}_x &= \begin{bmatrix} 1 & 0 & 0 \\ 0 & C_{\gamma_{\text{eh}}} & -S_{\gamma_{\text{eh}}} \\ 0 & S_{\gamma_{\text{eh}}} & C_{\gamma_{\text{eh}}} \end{bmatrix},
\end{aligned} \tag{3}
$$

where α_{eh}, β_{eh} and γ_{eh} represent the yaw, pitch and roll angles of the eye with respect to the head frame, respectively.

The rotation of f_e is represented by applying the above rotation matrices in Helmholtz sequence (Haslwanter, 1995) as

$$
{}^{h}\mathbf{F}_e = {}^{h}_{e}\mathbf{R}_y {}^{h}_{e}\mathbf{R}_z {}^{h}_{e}\mathbf{R}_x {}^{h}\mathbf{F}_{e0}, \tag{4}
$$

where $\mathbf{F}_{e0}$ is the initial and $\mathbf{F}_e$ is the rotated orientations for f_e. After substituting ${}^{h}\mathbf{y}_e$ and ${}^{h}\mathbf{z}_e$ into (2), the alignment A_{ep} is obtained as

$$
A_{\text{ep}} = (C_{\alpha_{\text{eh}}} + C_{\beta_{\text{eh}}}) C_{\gamma_{\text{eh}}} - S_{\alpha_{\text{eh}}} S_{\beta_{\text{eh}}} S_{\gamma_{\text{eh}}}. \tag{5}
$$

To achieve the maximum alignment between f_e and f_p at an arbitrary eye position, the redundant torsional rotation of an eye can be used to maximize A_{ep}. By setting the derivative of A_{ep} with respect to γ_{eh} to zero, we have

$$
\frac{\mathrm{d}A_{\text{ep}}}{\mathrm{d}\gamma_{\text{eh}}} = -\left(C_{\alpha_{\text{eh}}} + C_{\beta_{\text{eh}}}\right) S_{\gamma_{\text{eh}}} - S_{\alpha_{\text{eh}}} S_{\beta_{\text{eh}}} C_{\gamma_{\text{eh}}} = 0. \tag{6}
$$

Rearranging (6) for γ_{eh} gives

$$
\gamma_{\text{eh}} = \tan^{-1}\left(\frac{-S_{\alpha_{\text{eh}}} S_{\beta_{\text{eh}}}}{C_{\alpha_{\text{eh}}} + C_{\beta_{\text{eh}}}}\right). \tag{7}
$$

The above equation shows the Helmholtz-torsional angle required to maximize A_{ep} (2). This is the same as the Helmholtz-torsion required for L1 (von Helmholtz & Southall, 2005).

To further prove that (7) gives the maximum extreme, the second order derivative is obtained as

$$
\frac{\mathrm{d}^2 A_{\text{ep}}}{\mathrm{d}\gamma_{\text{eh}}^2} = -\left(C_{\alpha_{\text{eh}}} + C_{\beta_{\text{eh}}}\right) C_{\gamma_{\text{eh}}} + S_{\alpha_{\text{eh}}} S_{\beta_{\text{eh}}} S_{\gamma_{\text{eh}}}. \tag{8}
$$

By substituting (7) into (8), we have

$$
\frac{\mathrm{d}^2 A_{\text{ep}}}{\mathrm{d}\gamma_{\text{eh}}^2} = -\left(C_{\alpha_{\text{eh}}} + C_{\beta_{\text{eh}}}\right) C_{\gamma_{\text{eh}}} - \frac{S_{\alpha_{\text{eh}}}^2 S_{\beta_{\text{eh}}}^2 C_{\gamma_{\text{eh}}}}{C_{\alpha_{\text{eh}}} + C_{\beta_{\text{eh}}}}. \tag{9}
$$

As the eye movement is within either the first or fourth quadrant, Eq. (9) will be negative within its domain, which proves that Eq.(7) is a maximizer.

In the above, L1 is derived by maximizing the alignment (2) and this implies that, by following L1, the eye maintains the maximum alignment with the primary orientation f_p. The amount of tilt λ does not appear in (5). This suggests that f_p can be rotated from f_h by any angle λ without compromising L1.

3. Listing's law in saccades

L1 was originally proposed for eye fixations. It was later discovered that the L1 also holds during saccades (Tweed, Cadera, & Vilis, 1990; Tweed & Vilis, 1990). Consequently, the concept of single rotation in L1 is extended to saccades and the saccadic eye movements are often assumed to follow the geodesics on SO(3),[1] which can be represented by a fixed-axis rotation (Ghosh & Wijayasinghe, 2012; Ghosh, Wijayasinghe, & Kahagalage, 2014; Hepp, 1990, 1995; Novelia & O'Reilly, 2015a, 2015b). However, following L1 does not necessarily mean that the trajectory is a fixed-axis rotation. The eye is said to obey L1 as long as the torsion is fixed with respect to a given gaze position and this torsion has the same amount of angle as the torsion achieved by a single rotation from the primary position. Experiments also show that the trajectory of saccades is slightly deviated away from the fixed-axis rotations (Tweed et al., 1990; Tweed & Vilis, 1990).

In this section we show that the alignment equation can be extended to describe the trajectory of saccadic eye movements. The subscription eh and the superscription h are dropped in this section to simplify the notation as all the eye rotations in this section are described with respect to the head and all vectors are measured from the head frame. For example α_{eh}, β_{eh}, γ_{eh} and the gaze vector ${}^{h}\mathbf{x}_e$ are simplified to α, β, γ and $\mathbf{x}_e$, respectively.

In Section 2, we show that L1 can be derived by maximizing A_{ep} (2) for a given gaze direction. As L1 also holds during saccades, the maximum alignment A_{ep} achieved by L1, which is denoted as A_{L1}, can be calculated by substituting (7) into (5) as

$$
A_{\text{L1}} = \sqrt{(C_\alpha + C_\beta)^2 + S_\alpha^2 S_\beta^2}, \tag{10}
$$

where $A_{\text{L1}} > 0$ in the realistic eye movement range.

We assume that at any position during a saccade, A_{ep} is maximized to A_{L1} so that the eye orientation follows L1. According to (10), A_{L1} varies with respect to the gaze position. In fixation, L1 maximizes A_{ep} which indicates that the eye prefer to maintain at an orientation with A_{ep} as higher as possible. Therefore, it is tempting to hypothesize that the eye would also prefer to travel along a trajectory maintaining A_{L1} as higher as possible during saccades. That is, the eye may attempt to maximize the integral of A_{L1} along the saccadic path.

However, maximizing the integral of A_{L1} is not a proper mathematical formulation for saccades as the integral of A_{L1} can go to infinity by non-saccadic eye movements such as an infinite path; i.e. continuously detouring. The problem is better described if we assume that the eye attempts to minimize the integral of $1/A_{\text{L1}}$ along a saccadic path. The integral of $1/A_{\text{L1}}$ through a trajectory (denoted as S) between points P and Q can be expressed as

[1] SO(3) is the special orthogonal group in three-dimensional space, which is also called the three-dimensional rotation group (Gallier, 2001).

$$S = \int_{t_P}^{t_Q} \frac{1}{A_{L1}(\alpha(t), \beta(t))} \|\dot{\mathbf{x}}_e(t)\| \, dt. \tag{11}$$

$\dot{\mathbf{x}}_e$ is the time derivative of gaze vector in head. $\|\dot{\mathbf{x}}_e\|$ represents the Euclidean norm of $\dot{\mathbf{x}}_e$,

$$\|\dot{\mathbf{x}}_e\| = \sqrt{\dot{\mathbf{x}}_e \cdot \dot{\mathbf{x}}_e}. \tag{12}$$

The gaze vector $\mathbf{x}_e$ represented by Helmholtz coordinates α, β and γ is

$$\mathbf{x}_e = \begin{bmatrix} C_\alpha C_\beta \\ S_\alpha \\ -C_\alpha S_\beta \end{bmatrix}. \tag{13}$$

The velocity vector $\dot{\mathbf{x}}_e$ is

$$\dot{\mathbf{x}}_e = \begin{bmatrix} -S_\alpha C_\beta \dot{\alpha} - C_\alpha S_\beta \dot{\beta} \\ C_\alpha \dot{\alpha} \\ S_\alpha S_\beta \dot{\alpha} - C_\alpha C_\beta \dot{\beta} \end{bmatrix}. \tag{14}$$

Applying (12) to find the magnitude of $\dot{\mathbf{x}}_e$, yields

$$\|\dot{\mathbf{x}}_e\| = \sqrt{\dot{\alpha}^2 + C_\alpha^2 \dot{\beta}^2}. \tag{15}$$

In order to obtain the trajectory that minimizes S using Euler-Lagrange's equation, the Lagrangian needs to be differentiable. However, the (15) is not differentiable when $\dot{\alpha}$ and $\dot{\beta}$ are equal to zero. In order to get around the problem, we remove the time information by parameterizing S in terms of α

$$S = \int_{\alpha_P}^{\alpha_Q} \frac{1}{A_{L1}(\alpha, \beta(\alpha))} \left\| \frac{d\mathbf{x}_e(\alpha)}{d\alpha} \right\| d\alpha, \tag{16}$$

where

$$\left\| \frac{d\mathbf{x}_e}{d\alpha} \right\| = \sqrt{1 + C_\alpha^2 \beta'^2} \tag{17}$$

and

$$\beta' = \frac{d\beta}{d\alpha}.$$

The Euclidean norm (17) is now differentiable since it is always greater than zero. Substituting (10) and (17) to (16) gives

$$S = \int_{\alpha_P}^{\alpha_Q} \frac{\sqrt{1 + C_\alpha^2 \beta'^2}}{\sqrt{(C_\alpha + C_\beta)^2 + S_\alpha^2 S_\beta^2}} d\alpha. \tag{18}$$

The Lagrangian L_α is

$$L_\alpha = \frac{\sqrt{1 + C_\alpha^2 \beta'^2}}{\sqrt{(C_\alpha + C_\beta)^2 + S_\alpha^2 S_\beta^2}}. \tag{19}$$

Applying Euler-Lagrange's equation

$$\frac{d}{d\alpha}\left(\frac{\partial L_\alpha}{\partial \beta'}\right) - \frac{\partial L_\alpha}{\partial \beta} = 0,$$

we have

$$\begin{aligned} &-S_\beta - \beta'((2 + C_\alpha C_\beta)S_\alpha + C_\alpha^2 \beta'(S_\beta + S_\alpha \beta')) \\ &\quad + C_\alpha(1 + C_\alpha C_\beta)\beta'' = 0. \end{aligned} \tag{20}$$

With given boundary conditions α_P, β_P, α_Q and β_Q, (20) can be treated as a boundary value problem. Rewrite (20) as a system of two first-order ordinary differential equations (ODEs)

$$\begin{bmatrix} y_1' \\ y_2' \end{bmatrix} = \begin{bmatrix} y_2 \\ f(y_1, y_2) \end{bmatrix}, \tag{21}$$

where $y_1 = \beta$ and $y_2 = \beta'$. Using the boundary value problems solver, β and β' can be solved numerically in terms of α.

Parameterizing S in terms of α requires $\alpha_P \neq \alpha_Q$. When dealing with saccades that have $\alpha_P = \alpha_Q$, we can parameterize S in terms of β, which gives

$$S = \int_{\beta_P}^{\beta_Q} \frac{\sqrt{\alpha'^2 + C_\alpha^2}}{\sqrt{(C_\alpha + C_\beta)^2 + S_\alpha^2 S_\beta^2}} d\beta, \tag{22}$$

where

$$\alpha' = \frac{d\alpha}{d\beta}.$$

Since $-\pi/2 < \alpha < \pi/2$, $\sqrt{\alpha'^2 + C_\alpha^2}$ is differentiable in its domain. The Lagrangian L_β is

$$L_\beta = \frac{\sqrt{\alpha'^2 + C_\alpha^2}}{\sqrt{(C_\alpha + C_\beta)^2 + S_\alpha^2 S_\beta^2}}. \tag{23}$$

The Euler Lagrange equation in terms of β is

$$\frac{d}{d\beta}\left(\frac{\partial L_\beta}{\partial \alpha'}\right) - \frac{\partial L_\beta}{\partial \alpha} = 0,$$

which can be simplified to

$$\begin{aligned} &C_\alpha^2 S_\beta \alpha' + (2 + C_\alpha C_\beta) S_\alpha \alpha'^2 + S_\beta \alpha'^3 \\ &\quad + C_\alpha(C_\alpha S_\alpha + (1 + C_\alpha C_\beta)\alpha'') = 0. \end{aligned} \tag{24}$$

Let $y_1 = \alpha$ and $y_2 = \alpha'$ and rewrite (24) in the form of two ODEs as shown in (21), α and α' can be solved numerically in terms of β using a boundary value problems solver.

Since the trajectory that minimizes S between points $P(\alpha_P, \beta_P)$ and $Q(\alpha_Q, \beta_Q)$ is unique, (20) and (24) must give the same saccadic trajectory. Fig. 2 shows an example saccades between points $P(-19°, -13°)$ and $Q(16°, 18°)$, where the trajectories obtained from (20) and (24) are identical.

We used the boundary value problem solver *bvp4c* in Matlab[2] to compute 10 saccadic trajectories to demonstrate our approach. Fig. 3 shows the angles α and β of those trajectories. The blue trajectories are the saccades obtained by minimizing S where the red trajectories are the geodesic path between the corresponding initial and end position of the saccade. Trajectories 1–4 are four 20° saccades which take the gaze vector in clockwise direction (from the subject point of view) around a

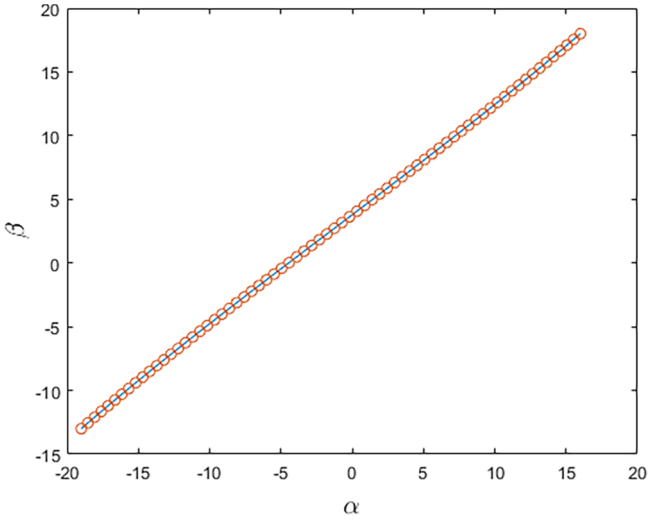

Fig. 2. Relation between α and β for boundary conditions of $P(-19°, -13°)$ and $Q(16°, 18°)$. The line is the results from (20) and the circles are the results from (24).

[2] Matlab function *bvp4c* solves boundary value problems for ordinary differential equations (https://mathworks.com/help/matlab/ref/bvp4c.html).

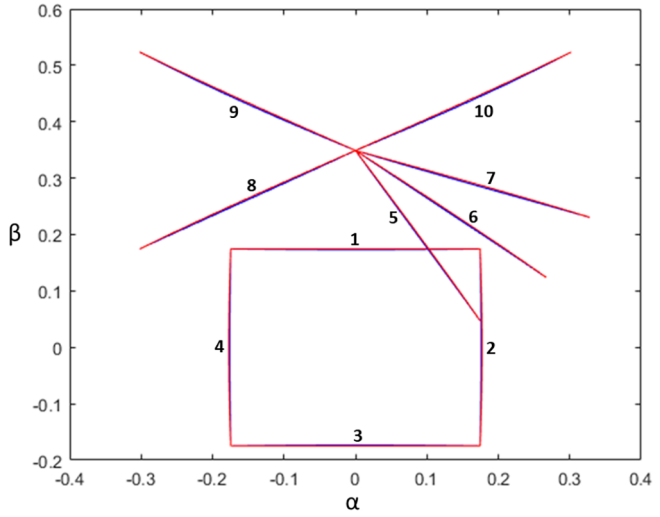

Fig. 3. The relationship between Helmholtz coordinates α and β for the ten saccades. The blue lines are the simulated saccadic trajectories and the red lines are the geodesics. (For interpretation of the references to colour in this figure legend, the reader is referred to the web version of this article.)

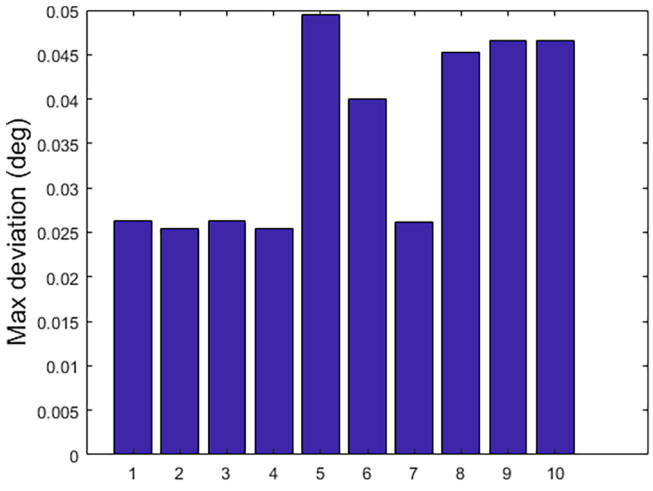

Fig. 4. The maximum absolute deviations between the geodesics and the simulated trajectories for the 10 saccades.

rectangle centered on primary position. 5–10 are saccades which departs from 20° down and move 20° amplitude to six different locations.

We have discussed that maximizing A_{ep} could indicate minimizing eye muscle stretches. In this context, a saccadic trajectory that minimizes S may achieve a minimum amount of muscle work. The saccadic trajectories that minimizes S are close to the geodesics on SO(3) as shown in Fig. 3.

Fig. 4 shows the maximum absolute deviations of the simulated saccadic trajectories to the corresponding geodesics. The deviation is defined as the angle between the gaze vector and the plane of the geodesics, where the gaze vector is calculated using (13). Although there exist small deviations between the geodesics and the simulated saccadic path, the deviations are too small to explain the curvature commonly observed in saccades (Ludwig & Gilchrist, 2002; Tweed et al., 1990; Tweed & Vilis, 1990). Therefore, our motor optimization equation does not address the deviations from geodesics in saccade, which supports the argument that those deviations are the result of neural programming (Van der Stigchel, Meeter, & Theeuwes, 2007a, 2007b).

The neural programming caused by shift of attention could be an explanation for these deviations in saccades. According to Rizzolatti, Riggio, Dascola, and Umiltá (1987), the shift of attention can be viewed as a by-product of the programming of an eye movement to a particular location. The programming of an eye movement towards a location generates an individual vector coding (Van der Stigchel, 2010; Van der Stigchel et al., 2007a). The change of attention at the moment that the eye movement is initiated activates two vector codings with one in the target location and the other in the location which attention is allocated. The averaged movement vector thus pointing to the intermediate location between the two. As the eye is instructed to move to the target, the vector coding to the attended location has to be inhibited during the mid-flight of the saccade and therefore, the saccadic trajectory deviates from the attended location (McSorley, Haggard, & Walker, 2004; Van der Stigchel, Meeter, & Theeuwes, 2007b).

4. Binocular extension of Listing's Law

The eye's orientation changes when the gaze direction converges to a near target, which is achieved by tilting the Listing's plane temporally about a quarter of the vergence angle (Minken & Van Gisbergen, 1994; Mok et al., 1992; Van Run & Van den Berg, 1993; Wong, 2004). This is known as the binocular extension of Listing's Law, often abbreviated as L2. As a result of L2, two eyes incyclorotate when looking up and excyclorotate when looking down, which is called as cyclovergence.

As discussed in the earlier section, L1 can be regarded as a result of motor optimization. In extending L1 to L2, another type of optimization plays an important role, which is the visual optimization (Tweed, 1997). The visual optimization in L2 refers to the optimization of images on two retinas. L2 maintains the correspondence of retinal images by reducing the migration of the epipolar lines during eye movement (Schreiber, Crawford, Fetter, & Tweed, 2001; Schreiber & Schor, 2007). Since the brain does not predict the change of epipolar geometry, optimizing the visual correspondence through L2 helps the brain to reduce the search zones of the corresponding image features, thereby reducing the computational load of the stereoscopic vision (Schreiber et al., 2001; Schreiber & Schor, 2007).

Experiments have shown that L2 maximizes retinal correspondence of target images by approximately equating Helmholtz-torsional angles between the left and right eyes (Tweed, 1997; Van Run & Van den Berg, 1993). Because the elevation plane of Helmholtz coordinates contains corresponding epipolar lines in the left and right images (Hansard & Horaud, 2010), the location of epipolar lines in the two retinal images are identical if the Helmholtz-torsional component of two eyes are the same. Therefore, by equating Helmholtz-torsional angles between two eyes, the brain is not required to search different zones of two images, which further lightening its computational load.

One thing worth to mention is that whether the visual optimization of L2 is visually mediated or non-visually mediated. The visually mediated visual optimization means that the eye rotations are elicited by images on retinas (Crone & Everhard-Halm, 1975; Hooge & Van den Berg, 2000). In L2, the eye rotations for visual optimization are the cyclovergences that reduce the cyclodisparity between the images on retinas. It was proved that cyclovergences caused by L2 do not rely on images on retinas by the experiments in the darkened environment (Minken & Van Gisbergen, 1994; Mok et al., 1992; Van Run & Van den Berg, 1993). Consequently, the torsional rotations of L2 are non-visually mediated.

The non-visually mediated visual optimization can be attributed to the adaptability of the oculomotor system. Adaption of the oculomotor system have been observed in the VOR (Clarke, Grigull, Mueller, & Scherer, 2000; Gonshor & Jones, 1976), eye gaze (Schmitz, Bock, Grigorova, & Ilieva, 2010) as well as cyclovergence (Taylor, Roberts, & Zee, 2000); therefore the non-visually mediated cyclovergence is likely to be a result of adapting to the visually mediated cyclovergence in the daily use of the eyes. The non-visually induced cyclovergence has the advantages of fast response and reduction in brain processing. The visually-induced cyclovergence is superimposed linearly on the non-

visually induced cyclovergence (Hooge & Van den Berg, 2000) to aid the visual optimization whenever necessary. For example, the visually mediated cyclovergence occurs when non-visually mediated cyclovergence does not provide sufficiently optimized image correspondences for stereo image fusion (Crone & Everhard-Halm, 1975; Van Rijn, Van der Steen, & Collewijn, 1992).

The question is how L2 contributes in maximizing the retinal correspondence of target images without utilizing visual information. The identical Helmholtz torsional coordinates between the two eyes (Tweed, 1997) is not a complete answer because it does not specify the exact amount of torsional rotations. We postulate that L2 maximizes the alignment between two eye frames (f_{el} and f_{er}) to reduce the retinal image disparity, which can be formulated as

$$A_{ee} = {}^{h}\mathbf{y}_{el}\cdot{}^{h}\mathbf{y}_{er} + {}^{h}\mathbf{z}_{el}\cdot{}^{h}\mathbf{z}_{er}. \tag{25}$$

In binocular vision, there are six Helmholtz coordinates, where α_{ehl} and α_{ehr} represent yaw rotations, β_{ehl} and β_{ehr} are pitch rotations, and γ_{ehl} and γ_{ehr} are roll rotations. An eye fixation defines the angles α_{ehl}, α_{ehr}, β_{ehl} and β_{ehr}. The torsional angles γ_{ehl}, γ_{ehr} can be fully defined through maximizing (25) and (2). In binocular vision, ${}^{h}\mathbf{y}_{e}$ and ${}^{h}\mathbf{z}_{e}$ in (2) are defined as

$${}^{h}\mathbf{y}_{e} = \frac{{}^{h}\mathbf{y}_{el} + {}^{h}\mathbf{y}_{er}}{|{}^{h}\mathbf{y}_{el} + {}^{h}\mathbf{y}_{er}|} \quad \text{and} \quad {}^{h}\mathbf{z}_{e} = \frac{{}^{h}\mathbf{z}_{el} + {}^{h}\mathbf{z}_{er}}{|{}^{h}\mathbf{z}_{el} + {}^{h}\mathbf{z}_{er}|}.$$

However, in near fixation, A_{ee} in (25) and A_{ep} in (2) cannot be maximized simultaneously as the global maximums of (25) and (2) are at different eye orientations. This implies that the visual optimization and the motor optimization compete each other in near fixation. It is known that the visually mediated cyclovergence that is elicited during dichoptic viewing compromises L1 (Crone & Everhard-Halm, 1975; Van Rijn et al., 1992), which suggests that the visual optimization has a higher priority than the motor optimization. Based on this, Eq.(25) is maximized first to solve the relationship between γ_{ehl} and γ_{ehr}. Based on the relation of γ_{ehl} and γ_{ehr}, the exact amounts of torsional angles are then calculated by maximizing Eq.(2).

As shown in Fig. 5, three angles θ, ϕ and v are used to define the binocular fixation (Van Run & Van den Berg, 1993), where θ is the angle between the line **ot** and the head transverse plane (the plane formed by $\mathbf{x}_h$ and $\mathbf{y}_h$). ϕ is the angle between the line **ot** and the head sagittal plane (the plane formed by $\mathbf{x}_h$ and $\mathbf{z}_h$). θ and ϕ define the direction of fixation in head (**ot**). The vergence angle (v) at fixation point is the angle formed by two eye gaze vectors, where v is defined to be negative for convergence (Minken & Van Gisbergen, 1994; Van Run & Van den Berg, 1993). The advantage of using θ, ϕ, and v to define the fixation of the eyes is to avoid the use of interocular distance because the interocular distance of each subject is different.

Using the rotation matrices in (3), the eye rotations under Helmholtz sequence can be expressed as

$${}^{h}\mathbf{F}_{el} = {}^{h}_{e}\mathbf{R}_{yle}\,{}^{h}\mathbf{R}_{zle}\,{}^{h}\mathbf{R}_{xl}\,{}^{h}\mathbf{F}_{el0}$$
$${}^{h}\mathbf{F}_{er} = {}^{h}_{e}\mathbf{R}_{yre}\,{}^{h}\mathbf{R}_{zre}\,{}^{h}\mathbf{R}_{xr}\,{}^{h}\mathbf{F}_{er0},$$

where ${}^{h}\mathbf{x}_{el0}$, ${}^{h}\mathbf{y}_{el0}$, ${}^{h}\mathbf{z}_{el0}$ and ${}^{h}\mathbf{x}_{er0}$, ${}^{h}\mathbf{y}_{er0}$, ${}^{h}\mathbf{z}_{er0}$ are same as ${}^{h}\mathbf{x}_{e0}$, ${}^{h}\mathbf{y}_{e0}$, ${}^{h}\mathbf{z}_{e0}$ as shown in (4). Gaze vector ${}^{h}\mathbf{x}_{el}$ and ${}^{h}\mathbf{x}_{er}$ are determined by the angles α_{ehl}, β_{ehl}, α_{ehr} and β_{ehr}, which are uniquely defined by angles θ, ϕ, and v.

The advantage of using Helmholtz sequence is that it naturally confines ${}^{h}\mathbf{x}_{el}$ and ${}^{h}\mathbf{x}_{er}$ on the same elevation, which can be written as

$$\beta_{ehl} = \beta_{ehr} = \tan^{-1}\left(\frac{S_\theta}{C_\theta C_\phi}\right). \tag{26}$$

The geometric relationship of fixation also gives

$$\frac{1}{2}\left(\frac{{}^{h}x_{el,2}}{{}^{h}x_{el,1}} + \frac{{}^{h}x_{er,2}}{{}^{h}x_{er,1}}\right) = \frac{C_\theta S_\phi}{C_\theta C_\phi}, \tag{27}$$

where $v_{\text{frame},i}$ represents the i−th element of the vector $\mathbf{v}_{\text{frame}}$. By

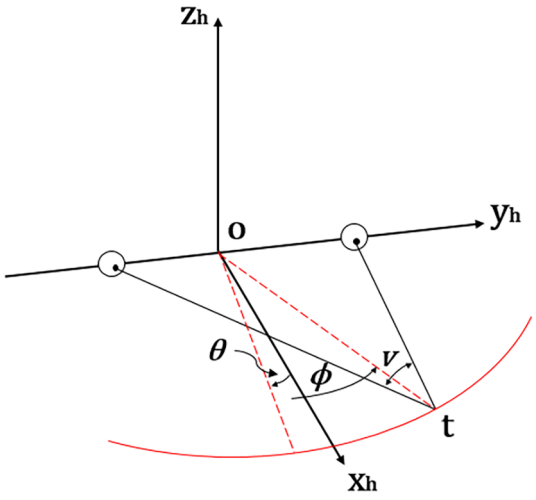

Fig. 5. Head frame for the binocular system (Redrawn from Van Run & Van den Berg, 1993).

rearranging (27), the relationship between α_{ehr} and α_{ehl} can be obtained as

$$\alpha_{ehr} = \tan^{-1}\left(2T_\phi C_{\beta_{ehr}} - \frac{T_{\alpha_{ehl}} C_{\beta_{ehr}}}{C_{\beta_{ehl}}}\right). \tag{28}$$

Since β_{ehl} and β_{ehr} are determined by (26) for given ϕ and θ, one more equation is needed to solve for α_{ehl}, and α_{ehr}. This equation can be derived using the vergence angle condition as

$$\mathbf{x}_{el}\cdot\mathbf{x}_{er} = \cos(-v). \tag{29}$$

Substituting (26) and (28) into (29) gives a complex equation with many trigonometric terms. As solving this equation for the analytical solution of α_{ehl} in terms of θ, ϕ and v is difficult, we compute α_{ehl} numerically for given θ, ϕ, and v angles.

Multiple solutions of α_{ehl} may exist due to the nature of the trigonometric terms. Since the eye movement is within first or fourth quadrants, the physically infeasible solutions with α_{ehl} smaller than − 90° or larger than 90° can be ignored. A pair of feasible solution can be found, one for α_{ehl} and the other one for α_{ehr}, where $\alpha_{ehl} < \alpha_{ehr}$.

The remaining unknowns are the torsional rotations γ_{ehl} and γ_{ehr}. We shall first maximize A_{ee} to find the relationship between γ_{ehl} and γ_{ehr}. Substituting α_{ehl}, α_{ehr}, β_{ehl} and β_{ehr} into (25) yields

$$A_{ee} = c_1 C_{(\gamma_{ehl}-\gamma_{ehr})} + c_2 S_{(\gamma_{ehl}-\gamma_{ehr})}, \tag{30}$$

where

$$c_1 = C_{\alpha_{ehl}} C_{\alpha_{ehr}} + C_{(\beta_{ehl}-\beta_{ehr})}(1 + S_{\alpha_{ehl}} S_{\alpha_{ehr}})$$
$$c_2 = -(S_{\alpha_{ehl}} + S_{\alpha_{ehr}}) S_{(\beta_{ehl}-\beta_{ehr})}.$$

In order to find the maximum of A_{ee} with respect to $\gamma_{ehl} - \gamma_{ehr}$, we compute

$$\frac{dA_{ee}}{d(\gamma_{ehl} - \gamma_{ehr})} = -c_1 S_{(\gamma_{ehl}-\gamma_{ehr})} + c_2 C_{(\gamma_{ehl}-\gamma_{ehr})} = 0. \tag{31}$$

Rearranging (31) gives the relationship between γ_{ehl} and γ_{ehr} as

$$\gamma_{ehl} = \tan^{-1}\left(\frac{c_2}{c_1}\right) + \gamma_{ehr}. \tag{32}$$

The second derivative of A_{ee} with respect to $\gamma_{ehl} - \gamma_{ehr}$ must be less than zero at this extreme if (32) gives the maximal A_{ee} not the minimal, which can be written as

$$\frac{d^2 A_{ee}}{d(\gamma_{ehl} - \gamma_{ehr})^2} = -c_1 C_{(\gamma_{ehl}-\gamma_{ehr})} - c_2 S_{(\gamma_{ehl}-\gamma_{ehr})} < 0. \tag{33}$$

Substituting (32) into (33) yields

$$-c_1\cos\left(\tan^{-1}\frac{c_2}{c_1}\right)-c_2\sin\left(\tan^{-1}\frac{c_2}{c_1}\right)<0. \tag{34}$$

Considering $\tan^{-1}\left(\frac{c_2}{c_1}\right)\in\left(-90°, 90°\right)$ and $c_1>0$, the above equation is simplified to

$$-1-\frac{c_2^2}{c_1^2}<0. \tag{35}$$

Since (35) always holds, (32) is proved to be the maximizer of A_{ee}.

Using the relationship between γ_{ehl} and γ_{ehr} in (32), the exact angles of γ_{ehl} and γ_{ehr} can be obtained by maximizing A_{ep}. This can be achieved by substituting (32) back to (2), which yields A_{ep} as a function of λ and γ_{ehr}. We shall set $\lambda=0$ here and we will later show that λ has no influence to the solutions. In oder to numerically find γ_{ehr} that maximizes A_{ep}, we used a pattern search algorithm[3] to find the minimizer of $-A_{ep}$.

The angle γ_{ehr} numerically found to minimize $-A_{ep}$ is equivalent to the angle that maximizes A_{ep}. By substituting this γ_{ehr} into (32), the corresponding value of γ_{ehl} can be determined. Once all eye rotation angles are calculated, the resultant eye rotation matrices for left and right eyes can be found as

$${}^{h}_{e}\mathbf{R}_{l}={}^{h}_{e}\mathbf{R}_{yl}{}^{h}_{e}\mathbf{R}_{zl}{}^{h}_{e}\mathbf{R}_{xl}\quad\text{and}\quad{}^{h}_{e}\mathbf{R}_{r}={}^{h}_{e}\mathbf{R}_{yr}{}^{h}_{e}\mathbf{R}_{zr}{}^{h}_{e}\mathbf{R}_{xr}.$$

The rotation vectors $\mathbf{r}_{ehl}$ and $\mathbf{r}_{ehr}$ corresponding to ${}^{h}_{e}\mathbf{R}_{l}$ and ${}^{h}_{e}\mathbf{R}_{r}$ can be calculated using (A.3).

By varying v from $-1°$ to $-29°$ with an increment of $-7°$, θ from to 25° with an increment of 2.5° and ϕ from $-35°$ to 35° with an increment of 2.5°, a total number of 3045 different eye fixations are simulated numerically. For each v, the Listing's planes of the left and right eyes are plotted using the tip of the rotation vectors $\mathbf{r}_{ehl}$ and $\mathbf{r}_{ehr}$.

Fig. 6 shows that Listing's planes are tilted temporally for both eyes, where r_y is the eye elevation and r_x is the eye torsion. The amount of tilt is approximately $\frac{v}{4}$ as shown in Fig. 7. The tilt angle of Listing's plane is obtained by first fitting the simulated data to

$$r_x=ar_y+br_z+c \tag{36}$$

using least squares. The angle of the plane temporal tilt is then calculated as the inverse tangent of the coefficient a.

It can be observed that when the vergence angle increases, Listing's planes become slightly more twisted. Experimentally measured Listing's planes are not ideal planes. These sets of measured data points deviate slightly from ideal planes, resulting in planes with "thickness" (Furman & Schor, 2003; Minken & Van Gisbergen, 1994; Van Run & Van den Berg, 1993). These deviations are attributed to the imperfect compliance of eye movements to L1 and the noise of experimental measurements. The small twist of LP shown in our simulation can be another factor that contributes to the deviation in eye vergence. More experiments with larger vergence angles may be able to validate the existence of the plane twist appearing in our simulations.

The raise of the tilt angle from $\frac{v}{4}$ for large vergence angles in Fig. 7 is mainly caused by the planar fit to the twist of the plane.

Rotation vectors $\mathbf{r}_{ehl}$ and $\mathbf{r}_{ehr}$ can be further divided into the conjugate component $\mathbf{s}$ and the disconjugate component $\mathbf{g}$ (Minken & Van Gisbergen, 1994; Mok et al., 1992; Van Run & Van den Berg, 1993). They are defined as

$$\mathbf{s}=\frac{\mathbf{r}_l+\mathbf{r}_r}{2}\quad\mathbf{g}=\frac{\mathbf{r}_l-\mathbf{r}_r}{2}. \tag{37}$$

Experiments in Mok et al. (1992), Van Run and Van den Berg (1993), and Minken and Van Gisbergen (1994) revealed that $\mathbf{s}$ and $\mathbf{g}$ are approximately given as

$$\mathbf{s}\approx\begin{bmatrix}0\\ \frac{\theta}{2}\\ \frac{\phi}{2}\end{bmatrix}\quad\mathbf{g}\approx\begin{bmatrix}\frac{\partial v}{8}\sim\frac{\partial v}{4}\\ 0\\ \frac{v}{4}\end{bmatrix}. \tag{38}$$

In order to obtain the $\mathbf{s}$ and $\mathbf{g}$ from our simulated results, linear regression is performed. Each element of $\mathbf{s}$ and $\mathbf{g}$ are regarded as dependent variables and various combinations of θ, ϕ and, v as independent variables. The R-squared value that represents the goodness of fitting is calculated for each linear regression. The independent variables that gives highest R-squared value in the linear regression are chosen to be the approximation to the corresponding dependent variable. The results suggest that

$$\mathbf{s}\approx\begin{bmatrix}0\\ \frac{\theta}{1.9}\\ \frac{\phi}{2}\end{bmatrix}\quad\mathbf{g}\approx\begin{bmatrix}\frac{\partial v}{7.1}\\ 0\\ \frac{v}{3.9}\end{bmatrix}. \tag{39}$$

The R-squared values of s_2, s_3, g_1 and g_3 of the approximations in (39) are 0.9990, 0.9992, 0.9931 and 0.9980 respectively, where v_i denotes the i-th element of a vector $\mathbf{v}$. For s_1 and g_2, the best approximations are zeros as s_1 has the mean and standard deviation of -1.139E^{-11} and -6.2961E^{-04} respectively. g_2 has its mean of 0 and standard deviation of 0.0021. Comparing (38) with (39), it can be observed that the results from the experiments are very close to the results from the simulation. This shows that maximizing the alignment between f_{el} and f_{er} and then the alignment between f_e and f_p in sequence gives the eye orientations following L2.

Since the maximization of the alignment between f_{el} and f_{er} is considered as a visual optimization and the maximization of the alignment between f_e and f_p is as a motor optimization, this can be viewed as another version of visual-motor hypothesis compared with Tweed, 1997. Our simulation results have non-zero Helmholtz-torsional angles but they are identical between two eyes. The mean and standard deviation of $|\gamma_{ehl}-\gamma_{ehr}|$ for our simulation are zero degrees, where the mean and standard deviation of $|\gamma_{ehl}|$ are 2.129° and 1.937° respectively.

In the above simulation result, we fixed $\lambda=0°$. By varying λ from 0° to 330° with an incremental of 30°, we find that there are no changes of the approximations of $\mathbf{s}$ and $\mathbf{g}$ compared with (39). This suggests that the amount of tilt λ between primary orientation and head frame has no influence on L2.

5. Monocular eye and head fixations

When gazing to a target, one can use the eye, the head, or the combination of two (Fetter et al., 1997). During the head-free eye gaze, the head movement contributes most of the horizontal rotation but less in vertical rotation, and it behaves like a Fick gimbal (Glenn & Vilis, 1992; Radau et al., 1994). The Fick gimbal-like behavior of the head is attributed to a motor optimization because the head takes more energy to pitch, which is due to the fact the center of mass of the head is located in front of the rotation axis. Therefore, the head moves like a Fick gimbal to reduce its vertical rotation (Fetter et al., 1997). The reduction of vertical rotation can be achieved by maintaining the alignment between head vertical axis and GIA, $\mathbf{z}_h\cdot\mathbf{z}_s$, where $\mathbf{z}_s$ points to the direction of GIA.

When the head moves, the vestibulo-ocular reflex (VOR), a compensatory eye movement, is elicited to stabilize eye gaze in space during translations and rotations of head (Raphan & Cohen, 2002). In this section, the static eye and head fixations are discussed, and therefore only the static lVOR affected by GIA is considered.

5.1. Equation of alignment extended for eye-head fixations

The eye fixation affected by lVOR shows a counterrolling phenomenon (Diamond, Markham, Simpson, & Curthoys, 1979; Hannen,

[3] Matlab function *patternsearch* is an optimization tool that able to find a local minimum of a function (https://mathworks.com/help/gads/patternsearch.html).

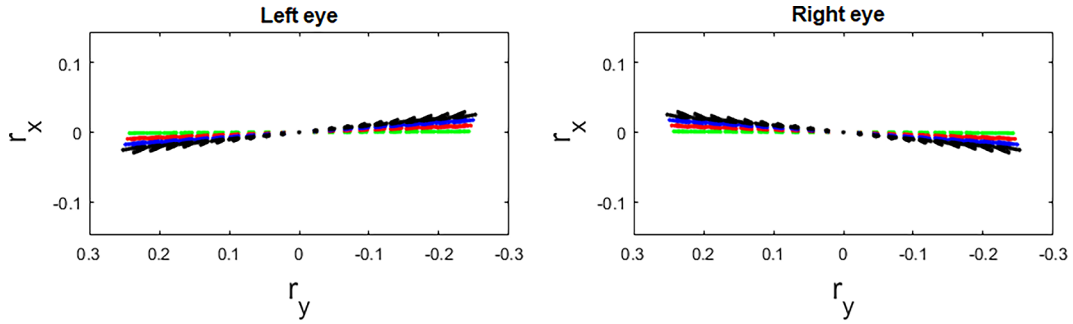

Fig. 6. Top view of Listing's plane for two eyes. The green, red, blue and black dots represent the Listing's plane at −1 degree, −8 degree, −15 degree and −22 degree of the vergence angle respectively. (For interpretation of the references to colour in this figure legend, the reader is referred to the web version of this article.)

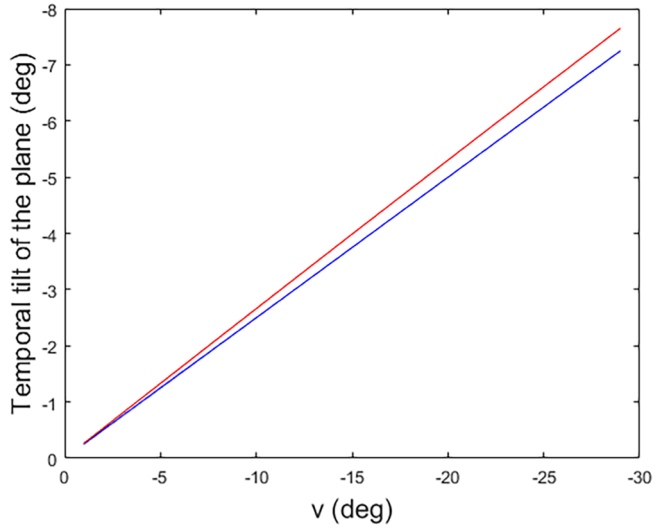

Fig. 7. Temporal tilt angles of Listing's plane as a function of eye vergence angle. The red line is tilt of Listing's plane from the simulation (angle of plane tilt for the left eye and the right eye are the same). The blue line is the $\frac{v}{4}$ approximation for the tilt of Listing's plane. (For interpretation of the references to colour in this figure legend, the reader is referred to the web version of this article.)

Kabrisky, Replogle, Hartzler, & Roccaforte, 1966; Miller, 1962). The purpose of the eye counterrolling is to rotate the eye vertical axis to align with GIA (Raphan & Cohen, 2002; Wearne, Raphan, & Cohen, 1999). The alignment between eye vertical axis and GIA can be represented as $\mathbf{z}_e \cdot \mathbf{z}_s$. However, maximizing $\mathbf{z}_e \cdot \mathbf{z}_s$ will result in eye movements that violate L1 when the head is fixed at upright position. Therefore, we propose that the lVOR attempts to maximize $\mathbf{y}_e \cdot \mathbf{y}_s + \mathbf{z}_e \cdot \mathbf{z}_s$ rather than $\mathbf{z}_e \cdot \mathbf{z}_s$. The head motor optimization represented by $\mathbf{z}_h \cdot \mathbf{z}_s$ and eye lVOR response by $\mathbf{y}_e \cdot \mathbf{y}_s + \mathbf{z}_e \cdot \mathbf{z}_s$ compromise L1 when the head moves. We postulate that the mixed objective between the eye motor optimization, the head motor optimization and the lVOR response is represented by the weighted sum of these alignments as

$$\begin{aligned}\widehat{A} = {}& {}^s\mathbf{y}_e \cdot {}^s\mathbf{y}_p + {}^s\mathbf{z}_e \cdot {}^s\mathbf{z}_p + k_1({}^s\mathbf{y}_e \cdot {}^s\mathbf{y}_s + {}^s\mathbf{z}_e \cdot {}^s\mathbf{z}_s) \\ & + k_2\, {}^s\mathbf{z}_h \cdot {}^s\mathbf{z}_s({}^s\mathbf{y}_e \cdot {}^s\mathbf{y}_s + {}^s\mathbf{z}_e \cdot {}^s\mathbf{z}_s) + k_3\, {}^s\mathbf{z}_h \cdot {}^s\mathbf{z}_s, \end{aligned} \tag{40}$$

where k_1, k_2, and k_3 are weighting factors, which have positive values. k_1 represents the effect of gravitational force on the alignment between the eye and the space. The size of k_1 is affected by the fact that the human eye has a larger ocular counterrolling under hyper-gravity and smaller counterrolling under hypo-gravity than that at 1 G (Cheung et al., 1992; Colenbrander, 1963; Diamond & Markham, 1988; Miller & Graybiel, 1970; Moore, Clément, Raphan, & Cohen, 2001). k_3 denotes the effect of gravitational force on the alignment between the head vertical axis and the spatial vertical axis. Since the motor optimization of the head becomes more crucial in environments with higher gravitational acceleration, k_3 becomes larger in such environments and smaller otherwise. The extra term $k_2\, {}^s\mathbf{z}_h \cdot {}^s\mathbf{z}_s({}^s\mathbf{y}_e \cdot {}^s\mathbf{y}_s + {}^s\mathbf{z}_e \cdot {}^s\mathbf{z}_s)$ is introduced to represent the coupling between the lVOR and the head motor optimization. More discussions on these weights will be provided in Section 5.2.

In fact, Eq.(40) is a generalized formulation of Eq.(2) and it is valid for L1 and L2 when the head is fixed at the upright position. In order to show that, let us assume that the head is held immobile at the upright position, which implies ${}^s\mathbf{y}_s = {}^s\mathbf{y}_h$ and ${}^s\mathbf{z}_s = {}^s\mathbf{z}_h$. Substituting these into Eq.(40) gives

$$\begin{aligned}\widehat{A} &= \mathbf{y}_{e_s} \cdot {}^s\mathbf{y}_p + {}^s\mathbf{z}_e \cdot {}^s\mathbf{z}_p + (k_1 + k_2)(\mathbf{y}_e^s \cdot {}^s\mathbf{y}_h + {}^s\mathbf{z}_e \cdot {}^s\mathbf{z}_h) + k_3 \\ &= \mathbf{y}_{e_s} \cdot [\mathbf{y}_p^s + (k_1 + k_2)\, {}^s\mathbf{y}_h] + {}^s\mathbf{z}_e \cdot [\mathbf{z}_p^s + (k_1 + k_2)\, {}^s\mathbf{z}_h] + k_3. \end{aligned} \tag{41}$$

Since k_3 does not affect the value of a maximizer of $\widehat{A}$, Eq.(41) can be viewed as the alignment between f_e and a frame which is compose of ${}^s\mathbf{y}_p + (k_1 + k_2)\, {}^s\mathbf{y}_h$ and ${}^s\mathbf{z}_p + (k_1 + k_2)\, {}^s\mathbf{z}_h$. The magnitudes of vectors ${}^s\mathbf{y}_p + (k_1 + k_2)\, {}^s\mathbf{y}_h$ and ${}^s\mathbf{z}_p + (k_1 + k_2)\, {}^s\mathbf{z}_h$ are equal and let us call it as m_r. If we define new unit vectors ${}^s\mathbf{y}_r$ and ${}^s\mathbf{z}_r$ as

$$\begin{aligned} m_r\, {}^s\mathbf{y}_r &= {}^s\mathbf{y}_p + (k_1 + k_2)\, {}^s\mathbf{y}_h \\ m_r\, {}^s\mathbf{z}_r &= {}^s\mathbf{z}_p + (k_1 + k_2)\, {}^s\mathbf{z}_h, \end{aligned} \tag{42}$$

then (41) can be written as

$$\widehat{A} = m_r({}^s\mathbf{y}_e \cdot {}^s\mathbf{y}_r + {}^s\mathbf{z}_e \cdot {}^s\mathbf{z}_r) + k_3. \tag{43}$$

Similar to k_3, m_r does not affect the maximizer of $\widehat{A}$. Therefore, only the alignment between the frame f_e and the frame f_r which is formed by ${}^s\mathbf{y}_r$ and ${}^s\mathbf{z}_r$ are important. Comparing f_r with f_p, the x axes of the two frames are pointing to the same direction, where the angle of f_r and f_p tilted from f_h are different.

In Sections 2 and 4, we have shown that the angle of tilt λ from f_h has no influence on L1 and L2, which means that the alignment between f_e and f_r has the same maximizer as the alignment between f_e and f_p. Therefore, maximizing (43) satisfies L1 and L2, which confirms that (40) is valid for L1 and L2 when the head is fixed at the upright position.

5.2. Static lVOR response

In order to show that Eq.(40) can be used to describe the eye-head gaze, it is necessary to determine the appropriate values for k_1, k_2 and k_3 in the normal gravity field. To begin with, the values of k_1, k_2 and k_3 are selected to satisfy a simple static lVOR response, the counterrolling (OCR).

The simulation of the eye-head coordination achieved by maximizing (40) begins with determining the initial eye orientation, which is the orientation when the gaze vector is at the primary position and the head is at its upright position. According to Eq.(43), the initial eye orientation ${}^s\mathbf{F}_{e0}$ at its primary position is coincident with the orientation

of f_r to achieve the maximized alignment of $\widehat{A}$, which yields

$$
{}^{s}\mathbf{x}_{e0}=\begin{bmatrix}1\\0\\0\end{bmatrix}\quad {}^{s}\mathbf{y}_{e0}=\begin{bmatrix}0\\ \frac{k_1+k_2+C_\lambda}{\sqrt{(1+(k_1+k_2)C_\lambda)^2+(-k_1-k_2)^2S_\lambda^2}}\\ \frac{S_\lambda}{\sqrt{(1+(k_1+k_2)C_\lambda)^2+(-k_1-k_2)^2S_\lambda^2}}\end{bmatrix}
$$

$$
{}^{s}\mathbf{z}_{e0}=\begin{bmatrix}0\\ \frac{-S_\lambda-2(k_1+k_2)C_\lambda S_\lambda}{\sqrt{(1+(k_1+k_2)C_\lambda)^2+(-k_1-k_2)^2S_\lambda^2}}\\ \frac{k_1+k_2+C_\lambda}{\sqrt{(1+(k_1+k_2)C_\lambda)^2+(-k_1-k_2)^2S_\lambda^2}}\end{bmatrix}. \tag{44}
$$

The OCR can be simulated by setting α_{eh}, β_{eh}, α_{hs} and β_{hs} equal to zero, as it only involves the eye and head rolling. The subscript eh, hs and es represent the rotations of the eye with respect to the head, the head with respect to the space and the eye with respect to the space, respectively.

The head rolling angle γ_{hs} is a given angle and the eye rolling angle γ_{eh} is unknown. The rotated eye orientation ${}^{s}\mathbf{F}_e$ and head orientation ${}^{s}\mathbf{F}_h$ can be calculated as

$$
\begin{aligned}
{}^{s}\mathbf{F}_e &= {}^{s}_{h}\mathbf{R}_{x}\,{}^{h}_{e}\mathbf{R}_{x}\,{}^{s}\mathbf{F}_{e0}\\
{}^{s}\mathbf{F}_h &= {}^{s}_{h}\mathbf{R}_{x}\,{}^{s}\mathbf{F}_{h0},
\end{aligned} \tag{45}
$$

where ${}^{s}\mathbf{F}_{h0}$ is the initial head orientations with ${}^{s}\mathbf{x}_{h0}=[1\ \ 0\ \ 0]^T$, ${}^{s}\mathbf{y}_{h0}=[0\ \ 1\ \ 0]^T$ and ${}^{s}\mathbf{z}_{h0}=[0\ \ 0\ \ 1]^T$. Substituting ${}^{s}\mathbf{y}_{s}=[0\ \ 1\ \ 0]^T$ and ${}^{s}\mathbf{z}_{s}=[0\ \ 0\ \ 1]^T$ along with ${}^{s}\mathbf{F}_e$ and ${}^{s}\mathbf{F}_h$ to (40), $\widehat{A}$ can be determined in terms of γ_{eh} and γ_{hs}. $\widehat{A}$ for OCR is represented in the form of

$$
\widehat{A}=\frac{\widehat{A}_{num}}{\widehat{A}_{den}}, \tag{46}
$$

where

$$
\begin{aligned}
\widehat{A}_{num} &= k_3 C_{\gamma_{hs}}\sqrt{1+(k_1+k_2)^2+2(k_1+k_2)C_\lambda}\\
&\quad+\{[2+k_2(k_1+k_2)]C_{\gamma_{eh}}+2k_1(k_1+k_2)C_{\gamma_{eh}+\gamma_{hs}}\\
&\quad+(k_1k_2+k_2^2)C_{\gamma_{eh}+2\gamma_{hs}}+2(k_1+k_2)C_{\gamma_{eh}-\lambda}+k_2C_{\gamma_{eh}+\lambda}\\
&\quad+2k_1C_{\gamma_{eh}+\gamma_{hs}+\lambda}+2k_2C_{\gamma_{eh}+2\gamma_{hs}+\lambda}\}
\end{aligned} \tag{47}
$$

and

$$
\widehat{A}_{den}=\sqrt{1+(k_1+k_2)^2+2(k_1+k_2)C_\lambda}. \tag{48}
$$

In order to find the γ_{eh} which maximize $\widehat{A}$, we let

$$
\frac{d\widehat{A}}{d\gamma_{eh}}=0. \tag{49}
$$

The OCR γ_{eh} that maximize $\widehat{A}$ can be calculated in terms of γ_{hs} as

$$
\gamma_{eh}=\tan^{-1}\left(\frac{\begin{aligned}&-2k_1(k_1+k_2)S_{\gamma_{hs}}-(k_1k_2+k_2^2)S_{2\gamma_{hs}}+(2k_1+k_2)S_\lambda\\&-2k_1S_{\gamma_{hs}+\lambda}-k_2S_{2\gamma_{hs}+\lambda}\end{aligned}}{\begin{aligned}&2+k_2(k_1+k_2)+2k_1(k_1+k_2)C_{\gamma_{hs}}+(k_1k_2+k_2^2)C_{2\gamma_{hs}}\\&+(2k_1+3k_2)C_\lambda+2k_1C_{\gamma_{hs}+\lambda}+k_2C_{2\gamma_{hs}+\lambda}\end{aligned}}\right) \tag{50}
$$

Now it is obvious that the weights k_1, k_2, k_3 and λ should be determined to compute the OCR. These values are tuned so that the OCR in Eq.(50) produces a similar path with one obtained from the experiment in the normal gravity field (Diamond et al., 1979; Hannen et al., 1966; Miller, 1962). By setting

$$
\begin{aligned}
k_1 &= 0.0981,\quad k_2=k_1/3,\quad k_3=0.981\\
\lambda &= -0.1\quad \text{radian},
\end{aligned} \tag{51}
$$

the OCR response that matches well with the experimental recording is achieved as shown in Fig. 8.

The angle $\lambda=-0.1$ radian is used to ensure that the OCR response is

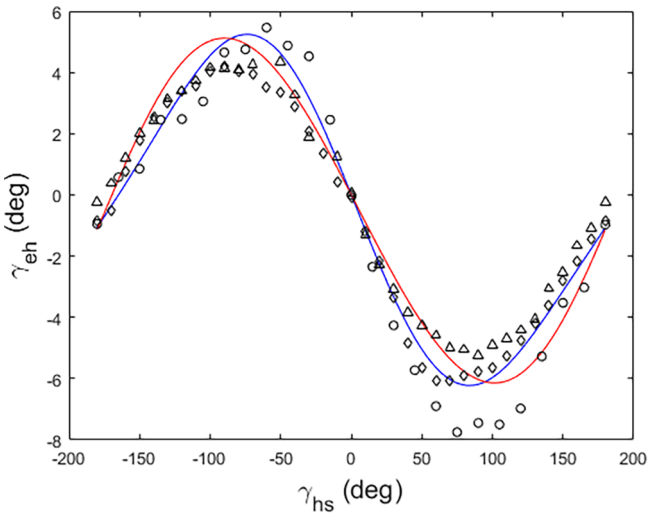

Fig. 8. OCR response with respect to head rolling. The blue curve is the OCR response using (51). The red curve is the OCR response when k_2 in (51) is 0. ◦ shows the OCR responses measured by Miller (1962). ◇ and △ are the OCR responses measured by Diamond et al. (1979), where ◇ shows the averaged OCR of the left and right eye for body rotations beginning right ear down and △ shows the averaged OCR of the left and right eye for body rotations beginning left ear down. (For interpretation of the references to colour in this figure legend, the reader is referred to the web version of this article.)

$-1°$ when the head is up-side-down ($\gamma_{eh}=180°$) as consistently observed in the experiments (Diamond et al., 1979; Hannen et al., 1966; Miller, 1962). This does not mean that the sinusoidal wave has a phase shift since the OCR response is 0° when the head is at upright position ($\gamma_{eh}=0°$).

The two peaks of OCR in Fig. 8 are 5.2427° and − 6.2246° which occur at − 74.0028° and 83.5606° of head rolling respectively. These characteristics are close to what were observed in Miller (1962), Hannen et al. (1966), Diamond et al. (1979).

The term related with k_2 represents that there is a coupling between the head orientation and the eye orientation. This makes the peaks of OCR happen at the absolute head rolling angles less than 90° as observed in experiments (Diamond et al., 1979; Hannen et al., 1966; Miller, 1962). The red curve in Fig. 8 shows that, with $k_2=0$, the two peaks of OCR occur at the absolute head rolling angles lager than 90°, which are − 90.0456° and 101.3223°.

The simulation result matches better with the experiment recording when this term is included. Further evidences are required to verify whether adding this term is reasonable.

To double check that the simulated OCR response is the maximizer of $\widehat{A}$, the second order derivative of $\widehat{A}$ with respect to γ_{eh} must less than zero, as

$$
\frac{d^2\widehat{A}}{d\gamma_{eh}^2}<0. \tag{52}
$$

Fig. 9 shows the second order derivative is negative for all γ_{eh}. This proves that the simulated OCR maximizes $\widehat{A}$.

To further validate Eq.(40) and the selected values of λ and k_i's, the orientations of LP during static head tilt are investigated. The derivation of the eye torsion γ_{eh} through maximizing $\widehat{A}$ can be found in Appendix B.

By varying α_{eh} and β_{eh} from − 35° to 35° with an increment of 2° for (B.3) and (B.6) respectively, Listing's plane of eye gazes under static head roll and under static head pitch using (51) are plotted as shown in Fig. 10. Furthermore, to ensure that (B.3) and (B.6) give the maximizer of $\widehat{A}$, Eq.(52) is numerically verified for each eye orientations but the plot is omitted for saving the space.

Fig. 10a shows that LP shifted to 0.0439 in r_x direction (5.0286°

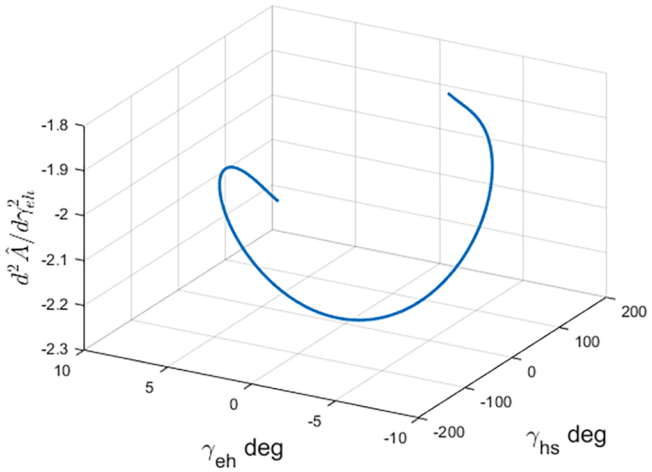

Fig. 9. The value of $d^2\widehat{A}/d\gamma_{eh}^2$ as a function of γ_{eh} and γ_{hs}, when (51) is used.

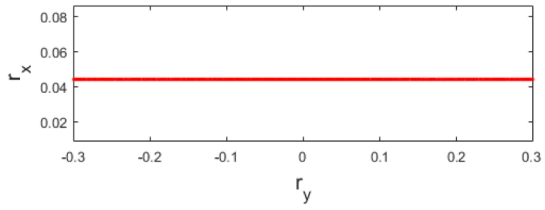

(a) Top view of rotation vector tips under −60° head rolling.

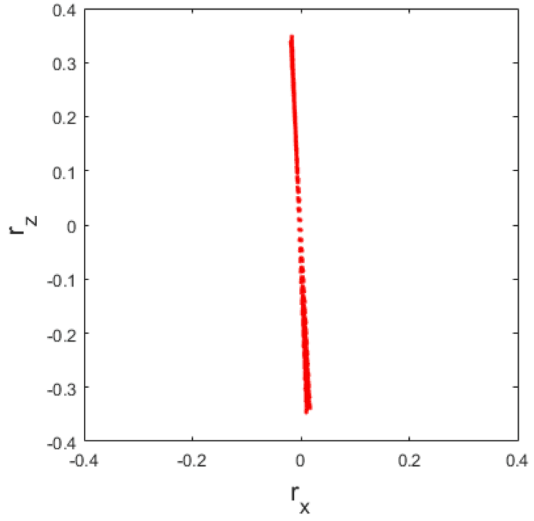

(b) Side view of rotation vector tips under 60° head pitching.

Fig. 10. Eye orientations under head tilt.

torsionally) under − 60° head roll, which is close to what is observed in both rhesus monkeys (Misslisch et al., 2001) and humans (Bockisch & Haslwanter, 2001). For orientation of LP during static head pitch, similar tilts in pitch of LP are observed in both monkeys and humans. However, the angle of tilt in humans is less than what is reported in monkeys (Bockisch & Haslwanter, 2001; Furman & Schor, 2003; Misslisch et al., 2001; Nooij et al., 2008). Fig. 10b shows the LP under 60° head pitch (nose down). The tilt angle of plane in pitch is calculated as the inverse tangent of the coefficient *b* of the planar fit as in Eq.(36). The amount of the pitch angle of the plane in Fig. 10b is approximately

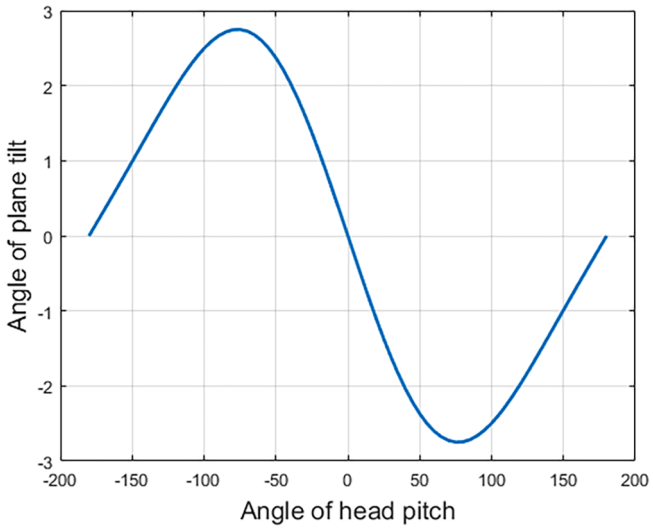

Fig. 11. Tilt of Listing's plane as a function of head pitch tilt.

2.6017° upward. This is close to what is observed in human (Bockisch & Haslwanter, 2001), which is an upward plane pitch about 2.928°.

Fig. 11 further illustrates the relationship between the tilt angle of plane and the pitch angle of head. The sinusoidal curve does not have an asymmetric behavior, which is different with observations in Haslwanter et al. (1992), Bockisch and Haslwanter (2001). The asymmetric behavior means that the tilt of LP when the head is erect is not equal to the tilt of LP when it is up-side-down. This is most likely because the primary position is assumed to be the direction of gazing straight ahead in our work. If the primary position is elevated so that the plane formed by $\mathbf{y}_p$ and $\mathbf{z}_p$ has nonzero backward tilt when the head is erect, the asymmetric behavior can be reproduced similar to the vector model as shown in Nooij et al. (2008).

5.3. Head-free eye gaze

To further justify (40) and the selected λ and k values. The head-free eye gazes are tested. The initial eye orientation ${}^{s}\mathbf{F}_{e0}$ and head orientation ${}^{s}\mathbf{F}_{h0}$ are the same as what was in Section 5.2. The rotated eye orientation in space and head orientation in space are therefore calculated as

$$
\begin{aligned}
{}^{s}\mathbf{F}_{e} &= {}^{s}_{e}\mathbf{R}_{ze}\,{}^{s}\mathbf{R}_{ye}\,{}^{s}\mathbf{R}_{x}\,{}^{s}\mathbf{F}_{e0}\\
{}^{s}\mathbf{F}_{h} &= {}^{s}_{h}\mathbf{R}_{zh}\,{}^{s}\mathbf{R}_{yh}\,{}^{s}\mathbf{R}_{x}\,{}^{s}\mathbf{F}_{h0}.
\end{aligned}
$$

Substituting ${}^{s}\mathbf{y}_s = [0\ \ 1\ \ 0]^T$ and ${}^{s}\mathbf{z}_s = [0\ \ 0\ \ 1]^T$ along with ${}^{s}\mathbf{F}_e$ and ${}^{s}\mathbf{F}_h$ to (40), $\widehat{A}$ can be represented in terms of α_{es}, β_{es}, γ_{es}, α_{hs}, β_{hs} and γ_{hs} as shown in Appendix C.

Note that Fick sequences are used to represent the eye and head rotations because the eye and head orientations in head-free eye gazes perform like the Fick gimbal (Glenn & Vilis, 1992; Radau et al., 1994). Using Fick coordinate is more intuitive to visualize if the angles of rotations generate orientations that are similar to those of the Fick gimbal.

α_{es} and β_{es} are given angles which define the target gaze direction in space. α_{hs}, β_{hs}, γ_{hs}, and γ_{es} are the unknown angles which need to be determined by maximizing $\widehat{A}$. Using the numerical optimization solver,[4] these angles can be determined simultaneously. The resultant rotation matrices for the eye and head in space can than be represented as

[4] a Matlab function *fmincon* is used, which is able to find the minimum of a constrained nonlinear multivariable function (https://mathworks.com/help/optim/ug/fmincon.html).

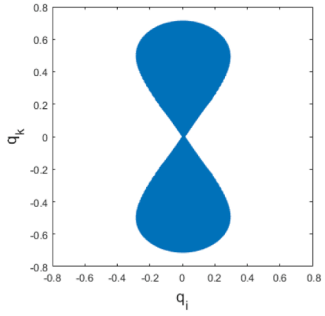

(a) Side view of quaternion vector tips for eye rotations in space (e_s).

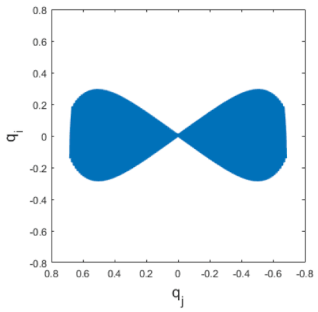

(b) Top view of quaternion vector tips for eye rotations in space (e_s).

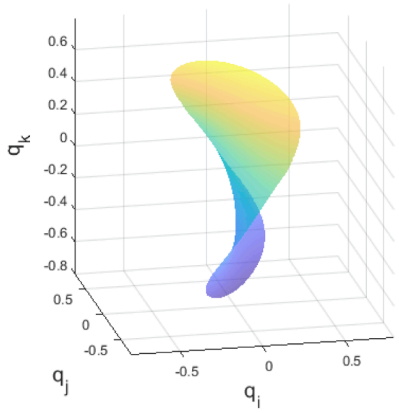

(c) 60% transparency 3D surface reconstructed from quaternion point clouds of eye rotations in space (e_s).

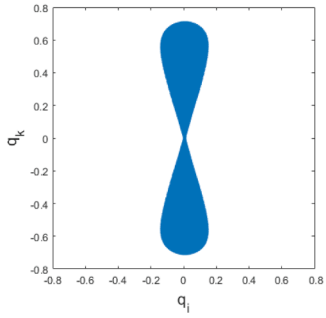

(d) Side view of quaternion vector tips for head rotations in space (h_s).

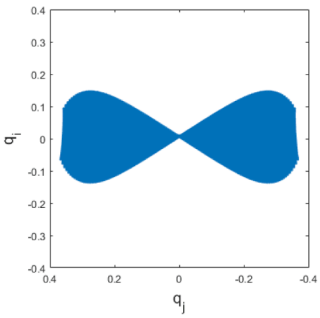

(e) Top view of quaternion vector tips for head rotations in space (h_s).

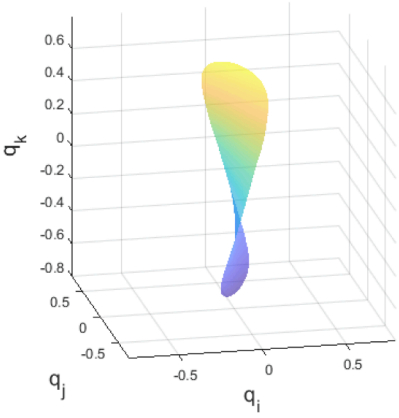

(f) 60% transparency 3D surface reconstructed from quaternion point clouds of head rotations in space (h_s).

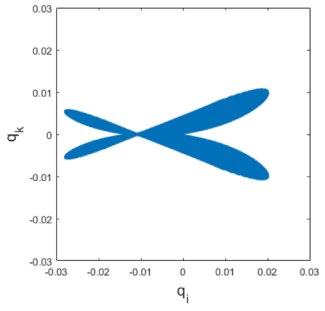

(g) Side view of quaternion vector tips for eye rotations in head (e_h).

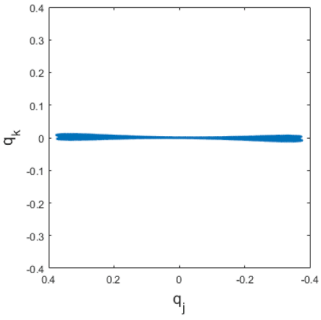

(h) Back view of quaternion vector tips for eye rotations in head (e_h).

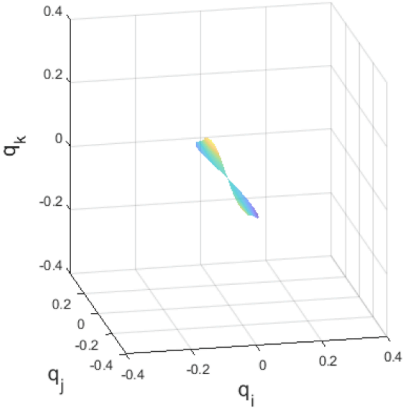

(i) 60% transparency 3D surface reconstructed from quaternion point clouds of eye rotations in head (e_h).

Fig. 12. Orientations of eye and head free gaze.

${}^{s}_{e}\mathbf{R} = {}^{s}_{e}\mathbf{R}_{ze}{}^{s}_{e}\mathbf{R}_{ye}{}^{s}_{e}\mathbf{R}_{x}$ and ${}^{s}_{h}\mathbf{R} = {}^{s}_{h}\mathbf{R}_{zh}{}^{s}_{h}\mathbf{R}_{yh}{}^{s}_{h}\mathbf{R}_{x}$.

The eye rotation in the head frame is

$$ {}^{h}_{e}\mathbf{R} = {}^{s}_{h}\mathbf{R}^{-1}{}^{s}_{e}\mathbf{R}. \tag{53} $$

The rotation represented by rotation matrices can be converted to quaternions using (A.1).

By varying α_{es} from $-90°$ to $90°$ with an incremental of $1°$ and β_{es} from $-85°$ to $85°$ with an incremental of $1°$, a total number of 30951 different head-free eye gaze positions are simulated. Fig. 12 shows the orientations of the eye in the space frame e_s, those of the head in the space frame h_s and the eye in the head frame e_h using the quaternions.

The e_s orientations in Fig. 12a–c form a twisted surface, which demonstrates that the eye movements obey Donders' Law. The twist of surface can be quantified using the following second order fitting function

$$q_i = a_1 + a_2 q_j + a_3 q_k + a_4 q_j^2 + a_5 q_j q_k + a_6 q_k^2. \tag{54}$$

The coefficient a_5 represents the amount of twist of the surface, which is defined as the twist score (Glenn & Vilis, 1992). The equation describing a gimbal system is

$$q_i = s(q_j q_k / q_r). \tag{55}$$

The coefficient s is the gimbal score, which is − 1 for a perfect Fick gimbal and 1 for a perfect Helmholtz gimbal (Glenn & Vilis, 1992). Our simulation suggests that e_s behaves like a Fick gimbal, which has a twist score of − 0.9816 and a gimbal score of − 0.7328. The values are close to but slightly larger than those observed in experiments (Glenn & Vilis, 1992; Radau et al., 1994). h_s also behaves like a Fick gimbal, where the twist score is − 0.8151 and the gimbal score is − 0.6834. These values are also similar to but slightly larger than what were observed in experiments (Glenn & Vilis, 1992; Radau et al., 1994).

The orientations of e_h are less clear compared with those of e_s and h_s. Both positive and negative twist scores for e_h surface were observed between subjects in experimental results (Glenn & Vilis, 1992). It is considered that the most appropriate surface fit for e_h is a first order one, since the standard deviation of surface fits between first, second and third order are similar (Radau et al., 1994).

Our simulation with 30,951 gaze positions gives the surface of e_h as shown in Fig. 12g–i. It can be observed that the eye mainly contributes to the vertical rotation, where the head dominates the horizontal and torsional rotations. The surface of e_h is not a flat plane even though the standard deviations for first (0.0111), second (0.0052) and third (0.0052) order fits are similar. In fact, the surface of e_h cannot be appropriately fitted by a single polynomial surface. The surface is more like a composition of the left (downward gaze) part and the right (upward gaze) part. Interestingly, the second order surface fitting for either the left part and the right part of e_h surface gives a twist score of − 17.78. However, the twist score for the fitting of entire surface is 10.83. This probably explains why both positive and negative twist scores are observed across subjects (Glenn & Vilis, 1992). Since there are only 5 target positions tested (Glenn & Vilis, 1992), it is possible that the variation of subjects' gazes during the test causes the surface inclination to one side and leads to a negative twist score.

In summary, the parameter values in (51) provide good approximations for the e_s and h_s orientations. The slightly larger twist scores and gimbal scores could probably due to the choice of k_i's, or the unmodeled functions such as cervical influence (Bles, Groen, Bos, De Jong, & Lok, 1998; Krejcova, Highstein, & Cohen, 1971). For e_h, we consider that the experiments in the literature do not have a sufficiently large number of target positions (5 target positions in Glenn & Vilis (1992) and 13 in Radau et al. (1994)) to reveal the precise shape of e_h surface. Experiments with more target gaze positions are required to validate our simulation results about e_h.

6. Conclusions

In this paper, we propose a method that utilizes the measurement of alignment between various coordinate frames to describe the kinematics of the eye and the eye-head movement. The alignment between the coordinate frames are quantified using the dot products of each frame's orthonormal unit vectors. The equations of the alignment are developed for the cases of L1, L2 and eye-head movements including head-free eye gazes and static lVORs. Our method provides a new framework for understanding the kinematic coordination between various eye and head functions.

In the future work, the current model will be extended to hypo and hyper gravity by relating the k_i's with gravitational constants and develop the equations to accommodate other eye functions such as aVOR. Also, more experimental validation of our results will be sought.

Acknowledgment

This research was supported by an Australian Government Research Training Program (RTP) Scholarship.

Appendix A. Quaternion and rotation vector

A rotation with a rotation matrix $\mathbf{R} \in \mathbb{R}^{3\times3}$ can be represented in a different form called quaternion $\mathbf{q}$ as

$$\begin{aligned} q_r &= \frac{\sqrt{1 + \mathrm{R}_{1,1} + \mathrm{R}_{2,2} + \mathrm{R}_{3,3}}}{2} \\ q_i &= \frac{\mathrm{R}_{3,2} - \mathrm{R}_{2,3}}{4q_r} \\ q_j &= \frac{\mathrm{R}_{1,3} - \mathrm{R}_{3,1}}{4q_r} \\ q_k &= \frac{\mathrm{R}_{2,1} - \mathrm{R}_{1,2}}{4q_r}, \end{aligned} \tag{A.1}$$

where $\mathrm{R}_{a,b}$ represents the element in a-th row and b-th column in the matrix $\mathbf{R}$ and

$$\mathbf{q} = \begin{bmatrix} q_r \\ q_i \\ q_j \\ q_k \end{bmatrix} = \begin{bmatrix} \cos(\rho/2) \\ n_x \sin(\rho/2) \\ n_y \sin(\rho/2) \\ n_z \sin(\rho/2) \end{bmatrix}. \tag{A.2}$$

Unit vector $\mathbf{n} = [n_x \;\; n_y \;\; n_z]^T$ is the axis of the rotation and ρ is the angle of the rotation. The rotation matrix $\mathbf{R}$ can also be represented in the form of a rotation vector $\mathbf{r}$ as

$$\mathbf{r} = \frac{1}{1 + \mathrm{R}_{1,1} + \mathrm{R}_{2,2} + \mathrm{R}_{3,3}} \begin{pmatrix} \mathrm{R}_{3,2} - \mathrm{R}_{2,3} \\ \mathrm{R}_{1,3} - \mathrm{R}_{3,1} \\ \mathrm{R}_{2,1} - \mathrm{R}_{1,2} \end{pmatrix}, \tag{A.3}$$

where $\mathbf{r} = \mathbf{n}\tan(\rho/2)$ (Haslwanter, 1995).

Appendix B. Eye torsion for head tilted eye gazes

When the head is tilted from the upright position at an roll angle, there are no yaw and pitch component of head rotation, which gives $\alpha_{\mathrm{hs}} = \beta_{\mathrm{hs}} = 0$. The head roll angle γ_{hs} is an independent variable which describes the amount of head roll. The yaw and pitch angle of the eye α_{eh} and β_{eh} are also independent variables which define the direction of eye gaze. The eye torsion γ_{eh} is an dependent variable that requires to maximize $\widehat{A}$. The rotated eye frame ${}^{\mathrm{s}}\mathbf{F}_e$ and head frame ${}^{\mathrm{s}}\mathbf{F}_h$ can be obtained as

$${}^{\mathrm{s}}\mathbf{F}_e = {}^{\mathrm{s}}_{h}\mathbf{R}_{xe}\,{}^{\mathrm{h}}\mathbf{R}_{ye}\,{}^{\mathrm{h}}\mathbf{R}_{ze}\,{}^{\mathrm{h}}\mathbf{R}_{x}\,{}^{\mathrm{s}}\mathbf{F}_{e0}$$

$${}^{\mathrm{s}}\mathbf{F}_h = {}^{\mathrm{s}}_{h}\mathbf{R}_{x}\,{}^{\mathrm{s}}\mathbf{F}_{h0}$$

where ${}^{\mathrm{s}}\mathbf{F}_{e0}$ and ${}^{\mathrm{s}}\mathbf{F}_{h0}$ are the same as used in (45). By substituting ${}^{\mathrm{s}}\mathbf{F}_e$ and ${}^{\mathrm{s}}\mathbf{F}_h$ with ${}^{\mathrm{s}}\mathbf{y}_{\mathrm{s}} = [0\ \ 1\ \ 0]^T$ and ${}^{\mathrm{s}}\mathbf{z}_{\mathrm{s}} = [0\ \ 0\ \ 1]^T$ into Eq.(40), $\widehat{A}$ for lVOR under head roll is derived in the form of $\widehat{A}_{num}/\widehat{A}_{den}$ same as in (46), where

$$\begin{aligned}\widehat{A}_{num} = {} & 2k_3C_{\gamma_{\mathrm{hs}}}\sqrt{1+(k_1+k_2)^2+2(k_1+k_2)C_\lambda} + (C_{\alpha_{\mathrm{eh}}}+C_{\beta_{\mathrm{eh}}})\{[2+k_2(k_1+k_2)]C_{\gamma_{\mathrm{eh}}} + 2k_1(k_1+k_2)C_{\gamma_{\mathrm{eh}}+\gamma_{\mathrm{hs}}} + (k_1k_2+k_2^2)C_{\gamma_{\mathrm{eh}}+2\gamma_{\mathrm{hs}}} + 2(k_1+k_2)C_{\gamma_{\mathrm{eh}}-\lambda} \\ & + k_2C_{\gamma_{\mathrm{eh}}+\lambda} + 2k_1C_{\gamma_{\mathrm{eh}}+\gamma_{\mathrm{hs}}+\lambda} + 2k_2C_{\gamma_{\mathrm{eh}}+2\gamma_{\mathrm{hs}}+\lambda}\} - S_{\alpha_{\mathrm{eh}}}S_{\beta_{\mathrm{eh}}}\{[2+k_2(k_1+k_2)]S_{\gamma_{\mathrm{eh}}} + 2k_1(k_1+k_2)S_{\gamma_{\mathrm{eh}}+\gamma_{\mathrm{hs}}} + (k_1k_2+k_2^2)S_{\gamma_{\mathrm{eh}}+2\gamma_{\mathrm{hs}}} + 2(k_1+k_2)S_{\gamma_{\mathrm{eh}}-\lambda} \\ & + k_2S_{\gamma_{\mathrm{eh}}+\lambda} + 2k_1S_{\gamma_{\mathrm{eh}}+\gamma_{\mathrm{hs}}+\lambda} + 2k_2S_{\gamma_{\mathrm{eh}}+2\gamma_{\mathrm{hs}}+\lambda}\}\end{aligned} \tag{B.1}$$

and

$$\widehat{A}_{den} = 2\sqrt{1+(k_1+k_2)^2+2(k_1+k_2)C_\lambda}. \tag{B.2}$$

The eye torsion γ_{eh} that maximizes $\widehat{A}$ can be determined using (49), which results in

$$\gamma_{\mathrm{eh}} = \tan^{-1}\left(\frac{\begin{array}{l}-\{[2+k_2(k_1+k_2)]+2k_1(k_1+k_2)C_{\gamma_{\mathrm{hs}}}+(k_1k_2+k_2^2)C_{2\gamma_{\mathrm{hs}}}+(2k_1+3k_2)C_\lambda+2k_1C_{\gamma_{\mathrm{hs}}+\lambda}+k_2C_{2\gamma_{\mathrm{hs}}+\lambda}\}S_{\alpha_{\mathrm{eh}}}S_{\beta_{\mathrm{eh}}} \\ -[2k_1(k_1+k_2)S_{\gamma_{\mathrm{hs}}}+(k_1k_2+k_2^2)S_{2\gamma_{\mathrm{hs}}}-(2k_1+k_2)S_\lambda+2k_1S_{\gamma_{\mathrm{hs}}+\lambda}+k_2S_{2\gamma_{\mathrm{hs}}+\lambda}](C_{\alpha_{\mathrm{eh}}}+C_{\beta_{\mathrm{eh}}})\end{array}}{\begin{array}{l}\{[2+k_2(k_1+k_2)]+2k_1(k_1+k_2)C_{\gamma_{\mathrm{hs}}}+(k_1k_2+k_2^2)C_{2\gamma_{\mathrm{hs}}}+(2k_1+3k_2)C_\lambda+2k_1C_{\gamma_{\mathrm{hs}}+\lambda}+k_2C_{2\gamma_{\mathrm{hs}}+\lambda}\}(C_{\alpha_{\mathrm{eh}}}+C_{\beta_{\mathrm{eh}}}) \\ -[2k_1(k_1+k_2)S_{\gamma_{\mathrm{hs}}}+(k_1k_2+k_2^2)S_{2\gamma_{\mathrm{hs}}}-(2k_1+k_2)S_\lambda+2k_1S_{\gamma_{\mathrm{hs}}+\lambda}+k_2S_{2\gamma_{\mathrm{hs}}+\lambda}]S_{\alpha_{\mathrm{eh}}}S_{\beta_{\mathrm{eh}}}.\end{array}}\right) \tag{B.3}$$

When the head is tilted from the upright position at a pitch angle, the only difference to the case of head roll is that $\gamma_{\mathrm{hs}} = 0$ and β_{hs} is an independent variable that describes the amount of head pitch. Thus the rotated eye frame ${}^{\mathrm{s}}\mathbf{F}_e$ and the head frame ${}^{\mathrm{s}}\mathbf{F}_h$ in this case become

$$\begin{aligned}{}^{\mathrm{s}}\mathbf{F}_e &= {}^{\mathrm{s}}_{h}\mathbf{R}_{ye}\,{}^{\mathrm{h}}\mathbf{R}_{ye}\,{}^{\mathrm{h}}\mathbf{R}_{ze}\,{}^{\mathrm{h}}\mathbf{R}_{x}\,{}^{\mathrm{s}}\mathbf{F}_{e0} \\ {}^{\mathrm{s}}\mathbf{F}_h &= {}^{\mathrm{s}}_{h}\mathbf{R}_{y}\,{}^{\mathrm{s}}\mathbf{F}_{h0}.\end{aligned}$$

Inserting ${}^{\mathrm{s}}\mathbf{F}_e$ and ${}^{\mathrm{s}}\mathbf{F}_h$ with ${}^{\mathrm{s}}\mathbf{y}_{\mathrm{s}} = [0\ \ 1\ \ 0]^T$ and ${}^{\mathrm{s}}\mathbf{z}_{\mathrm{s}} = [0\ \ 0\ \ 1]^T$ in (40) gives $\widehat{A}$ for lVOR under head pitching as

$$\begin{aligned}\widehat{A}_{num} = {} & 2C_{\alpha_{\mathrm{eh}}}C_{\gamma_{\mathrm{eh}}} + 2k_1^2C_{\beta_{\mathrm{eh}}+\beta_{\mathrm{hs}}}C_{\gamma_{\mathrm{eh}}} + 2k_3C_{\beta_{\mathrm{hs}}}\sqrt{1+(k_1+k_2)^2+2(k_1+k_2)C_\lambda} + 2C_{\alpha_{\mathrm{eh}}}\{C_{\gamma_{\mathrm{eh}}}[(k_1+k_2)(k_1+k_2C_{\beta_{\mathrm{hs}}})+2k_1C_\lambda] + k_2(C_{\gamma_{\mathrm{eh}}-\lambda}+C_{\beta_{\mathrm{hs}}}C_{\gamma_{\mathrm{eh}}+\lambda})\} \\ & - 2k_1C_{\gamma_{\mathrm{eh}}+\lambda}S_{\beta_{\mathrm{eh}}}S_{\beta_{\mathrm{hs}}} - 2S_{\alpha_{\mathrm{eh}}}S_{\beta_{\mathrm{eh}}}S_{\gamma_{\mathrm{eh}}} - 2k_1^2S_{\alpha_{\mathrm{eh}}}S_{\beta_{\mathrm{eh}}+\beta_{\mathrm{hs}}}S_{\gamma_{\mathrm{eh}}} + 2k_2^2C_{\beta_{\mathrm{hs}}}(C_{\beta_{\mathrm{eh}}+\beta_{\mathrm{hs}}}C_{\gamma_{\mathrm{eh}}} - S_{\alpha_{\mathrm{eh}}}S_{\beta_{\mathrm{eh}}+\beta_{\mathrm{hs}}}S_{\gamma_{\mathrm{eh}}}) - 2k_1S_{\alpha_{\mathrm{eh}}}S_{\beta_{\mathrm{eh}}}S_{\gamma_{\mathrm{eh}}-\lambda} \\ & + k_2S_{\beta_{\mathrm{eh}}}\{-C_{\gamma_{\mathrm{eh}}+\lambda}S_{2\beta_{\mathrm{hs}}} - [k_1+2k_1C_{\beta_{\mathrm{hs}}}+3C_\lambda+C_{2\beta_{\mathrm{hs}}}(k_1+C_\lambda)]S_{\alpha_{\mathrm{eh}}}S_{\gamma_{\mathrm{eh}}} - 2(1+C_{\beta_{\mathrm{hs}}})C_{\gamma_{\mathrm{eh}}}(k_1S_{\beta_{\mathrm{hs}}} - 2S_{\alpha_{\mathrm{eh}}}S^2_{\beta_{\mathrm{hs}}/2}S_\lambda)\} - 2k_1S_{\alpha_{\mathrm{eh}}}S_{\beta_{\mathrm{eh}}+\beta_{\mathrm{hs}}}S_{\gamma_{\mathrm{eh}}+\lambda} \\ & + C_{\beta_{\mathrm{eh}}}\{C_{\gamma_{\mathrm{eh}}}[2+k_1k_2+2k_1C_\lambda+3k_2C_\lambda+k_2C_{2\beta_{\mathrm{hs}}}(k_1+C_\lambda)+2k_1C_{\beta_{\mathrm{hs}}}(k_2+C_\lambda)] + 2(k_1-k_1C_{\beta_{\mathrm{hs}}}+k_2S^2_{\beta_{\mathrm{hs}}})S_{\gamma_{\mathrm{eh}}}S_\lambda \\ & + k_2S_{\alpha_{\mathrm{eh}}}[-2k_1(1+C_{\beta_{\mathrm{hs}}})S_{\beta_{\mathrm{hs}}}S_{\gamma_{\mathrm{eh}}} - S_{2\beta_{\mathrm{hs}}}S_{\gamma_{\mathrm{eh}}+\lambda}]\}\end{aligned} \tag{B.4}$$

and

$$\widehat{A}_{den} = 2\sqrt{1+(k_1+k_2)^2+2(k_1+k_2)C_\lambda}. \tag{B.5}$$

Using (49), the eye torsion γ_{hs} that maximizes $\widehat{A}$ of free eye gazes under static head pitch is derived as

$$\gamma_{\mathrm{eh}} = \tan^{-1}\left(\frac{\begin{array}{l}-2S_{\alpha_{\mathrm{eh}}}S_{\beta_{\mathrm{eh}}} - 2k_1C_\lambda S_{\alpha_{\mathrm{eh}}}(S_{\beta_{\mathrm{eh}}}+S_{\beta_{\mathrm{eh}}+\beta_{\mathrm{hs}}}) - 2(k_1^2+k_2^2S_{\beta_{\mathrm{hs}}})S_{\alpha_{\mathrm{eh}}}S_{\beta_{\mathrm{eh}}+\beta_{\mathrm{hs}}} - [2k_1k_2(1+C_{\beta_{\mathrm{hs}}})S_{\beta_{\mathrm{hs}}}+k_2C_\lambda S_{2\beta_{\mathrm{hs}}}]S_{\alpha_{\mathrm{eh}}}C_{\beta_{\mathrm{eh}}} \\ +2(k_1-k_1C_{\beta_{\mathrm{hs}}}+k_2S\beta^2_{\mathrm{hs}})S_\lambda C_{\beta_{\mathrm{eh}}} + 2k_1S_{\beta_{\mathrm{eh}}}S_{\beta_{\mathrm{hs}}}S_\lambda - k_2[k_1+2k_1C_{\beta_{\mathrm{hs}}}+3C_\lambda+C_{2\beta_{\mathrm{hs}}}(k_1+C_\lambda)]S_{\alpha_{\mathrm{eh}}}S_{\beta_{\mathrm{eh}}} + k_2S_{\beta_{\mathrm{eh}}}S_{2\beta_{\mathrm{hs}}}S_\lambda \\ +2k_2C_{\beta_{\mathrm{eh}}}S_\lambda(1-C_{\beta_{\mathrm{hs}}})\end{array}}{\begin{array}{l}2k_1S_\lambda S_{\alpha_{\mathrm{eh}}}(S_{\beta_{\mathrm{eh}}}-S_{\beta_{\mathrm{eh}}+\beta_{\mathrm{hs}}}) + 2C_{\alpha_{\mathrm{eh}}} + 2(k_1^2+k_2^2C_{\beta_{\mathrm{hs}}})C_{\beta_{\mathrm{eh}}+\beta_{\mathrm{hs}}} - k_2S_{2\beta_{\mathrm{hs}}}(C_{\beta_{\mathrm{eh}}}S_{\alpha_{\mathrm{eh}}}S_\lambda + S_{\beta_{\mathrm{eh}}}C_\lambda) \\ +[2+k_1k_2+2k_1C_\lambda+3k_2C_\lambda+k_2C_{2\beta_{\mathrm{hs}}}(k_1+C_\lambda)+2k_1C_{\beta_{\mathrm{hs}}}(k_2+C_\lambda)]C_{\beta_{\mathrm{eh}}} - 2k_1S_{\beta_{\mathrm{eh}}}S_{\beta_{\mathrm{hs}}}C_\lambda \\ -2k_2S_{\beta_{\mathrm{eh}}}(1+C_{\beta_{\mathrm{hs}}})(k_1S_{\beta_{\mathrm{hs}}}-2S_{\alpha_{\mathrm{eh}}}S^2_{\beta_{\mathrm{eh}}/2}S_\lambda) + 2C_{\alpha_{\mathrm{eh}}}[(k_1+k_2)(k_1+k_2C_{\beta_{\mathrm{hs}}})+2k_1C_\lambda] + 2k_2C_{\alpha_{\mathrm{eh}}}C_\lambda(1+C_{\beta_{\mathrm{hs}}})\end{array}}\right) \tag{B.6}$$

Appendix C. $\widehat{A}$ for Head-free eye gaze

The alingment equation $\widehat{A}$ for head-free eye gazes is shown in the form of numerator over denominator as in (46), where

$$\begin{aligned}\widehat{A}_{num} = {} & C_{\beta_{\mathrm{hs}}}C_{\beta_{\mathrm{es}}}[C_{\gamma_{\mathrm{hs}}-\gamma_{\mathrm{es}}}+(k_1+k_2)C_{\gamma_{\mathrm{hs}}-\gamma_{\mathrm{es}}+\lambda}] + S_{\alpha_{\mathrm{hs}}}\{[C_{\gamma_{\mathrm{hs}}-\gamma_{\mathrm{es}}}+(k_1+k_2)C_{\gamma_{\mathrm{hs}}-\gamma_{\mathrm{es}}+\lambda}]S_{\alpha_{\mathrm{es}}}[1+S_{\beta_{\mathrm{hs}}}S_{\beta_{\mathrm{es}}}] + C_{\alpha_{\mathrm{es}}}[S_{\beta_{\mathrm{hs}}}+S_{\beta_{\mathrm{es}}}]S_{\gamma_{\mathrm{hs}}-\gamma_{\mathrm{es}}}\} \\ & + C_{\alpha_{\mathrm{hs}}}\{C_{\alpha_{\mathrm{es}}}[C_{\gamma_{\mathrm{hs}}-\gamma_{\mathrm{es}}}+(k_1+k_2)C_{\gamma_{\mathrm{hs}}\gamma_{\mathrm{es}}+\lambda}][1+S_{\beta_{\mathrm{hs}}}S_{\beta_{\mathrm{es}}}] - S_{\alpha_{\mathrm{es}}}[S_{\beta_{\mathrm{hs}}}+S_{\beta_{\mathrm{es}}}]S_{\gamma_{\mathrm{hs}}-\gamma_{\mathrm{es}}}\} + (k_1+k_2)S_{\alpha_{\mathrm{hs}}-\alpha_{\mathrm{es}}}[S_{\beta_{\mathrm{hs}}}+S_{\beta_{\mathrm{es}}}]S_{\gamma_{\mathrm{hs}}-\gamma_{\mathrm{es}}+\lambda} \\ & + [k_1+k_2C_{\beta_{\mathrm{hs}}}C_{\gamma_{\mathrm{hs}}}]\{[C_{\alpha_{\mathrm{es}}}+C_{\beta_{\mathrm{es}}}][(k_1+k_2)C_{\gamma_{\mathrm{es}}}+C_{\gamma_{\mathrm{es}}+\lambda}] + S_{\alpha_{\mathrm{es}}}S_{\beta_{\mathrm{es}}}[(k_1+k_2)S_{\gamma_{\mathrm{es}}}+S_{\gamma_{\mathrm{es}}+\lambda}]\}\end{aligned} \tag{C.1}$$

and

$$\widehat{A}_{den} = \sqrt{1 + (k_1 + k_2)^2 + 2(k_1 + k_2)C_\lambda} + k_3 C_{\beta_{\text{hs}}} C_{\gamma_{\text{hs}}}. \tag{C.2}$$

References

Angelaki, D. E., Zhou, H.-H., & Wei, M. (2003). Foveal versus full-field visual stabilization strategies for translational and rotational head movements. *The Journal of Neuroscience, 23*(4), 1104–1108.

Bles, W., Groen, E., Bos, J. E., De Jong, V., & Lok, J. (1998). Cervically induced ocular torsion: Physiological and clinical aspects. *Acta oto-laryngologica, 118*(5), 613–617.

Bockisch, C. J., & Haslwanter, T. (2001). Three-dimensional eye position during static roll and pitch in humans. *Vision Research, 41*(16), 2127–2137.

Cheung, B., Money, K., Howard, I., Kirienko, N., Johnson, W., Lackner, J., ... Evanoff, J. (1992). Human ocular torsion during parabolic flights: an analysis with scleral search coil. *Experimental Brain Research, 90*(1), 180–188.

Clarke, A., Grigull, J., Mueller, R., & Scherer, H. (2000). The three-dimensional vestibulo-ocular reflex during prolonged microgravity. *Experimental Brain Research, 134*(3), 322–334.

Clarke, A. H., & Haslwanter, T. (2007). The orientation of listing's plane in microgravity. *Vision Research, 47*(25), 3132–3140.

Cohen, B., & Raphan, T. (2004). The physiology of the vestibuloocular reflex (vor). *The vestibular system* (pp. 235–285). Springer.

Colenbrander, A. (1963). The influence of g-forces on the counter-rolling of the eye. *Ophthalmologica, 146*(5), 309–313.

Crane, B. T., Tian, J., & Demer, J. L. (2006). Temporal dynamics of ocular position dependence of the initial human vestibulo-ocular reflex. *Investigative Ophthalmology & Visual Science, 47*(4), 1426–1438.

Crawford, J., & Vilis, T. (1991). Axes of eye rotation and listing's law during rotations of the head. *Journal of Neurophysiology, 65*(3), 407–423.

Crone, R., & Everhard-Halm, Y. (1975). Optically induced eye torsion. *Albrecht von Graefes Archiv für klinische und experimentelle Ophthalmologie, 195*(4), 231–239.

Demer, J. L., Oh, S. Y., & Poukens, V. (2000). Evidence for active control of rectus extraocular muscle pulleys. *Investigative Ophthalmology & Visual Science, 41*(6), 1280–1290.

Diamond, S. G., & Markham, C. H. (1988). Ocular torsion in upright and tilted positions during hypo-and hypergravity of parabolic flight. *Aviation, Space, and Environmental Medicine*.

Diamond, S. G., Markham, C. H., Simpson, N. E., & Curthoys, I. S. (1979). Binocular counterrolling in humans during dynamic rotation. *Acta oto-laryngologica, 87*(3–6), 490–498.

Donders, F. (1848). Beitrag zur lehre von den bewegungen des menschlichen auges. *Holland Beitr Anat Physiol Wiss, 1*(104), 384.

Ferman, L., Collewijn, H., & Van den Berg, A. (1987). A direct test of listing's law–i. Human ocular torsion measured in static tertiary positions. *Vision Research, 27*(6), 929–938.

Fetter, M., Haslwanter, T., Misslich, H., & Tweed, D. (1997). *Three-dimensional kinematics of the eye, head and limb movements.* CRC Press.

Furman, J. M., & Schor, R. H. (2003). Orientation of listing's plane during static tilt in young and older human subjects. *Vision Research, 43*(1), 67–76.

Gallier, J. (2001). The Quaternions and the Spaces S^3, SU(2), SO(3), and $\mathbb{RP}^3$. *Geometric methods and applications* (pp. 248–266). Springer.

Ghasia, F. F., & Angelaki, D. E. (2005). Do motoneurons encode the noncommutativity of ocular rotations? *Neuron, 47*(2), 281–293.

Ghosh, B. K., & Wijayasinghe, I. B. (2012). Dynamics of human head and eye rotations under donders' constraint. *IEEE Transactions on Automatic Control, 57*(10), 2478–2489.

Ghosh, B. K., Wijayasinghe, I. B., & Kahagalage, S. D. (2014). A geometric approach to head/eye control. *IEEE Access, 2*, 316–332.

Glenn, B., & Vilis, T. (1992). Violations of listing's law after large eye and head gaze shifts. *Journal of Neurophysiology, 68*(1), 309–318.

Gonshor, A., & Jones, G. M. (1976). Extreme vestibulo-ocular adaptation induced by prolonged optical reversal of vision. *The Journal of Physiology, 256*(2), 381–414.

Hannen, R., Kabrisky, M., Replogle, C., Hartzler, V., & Roccaforte, P. (1966). Experimental determination of a portion of the human vestibular system response through measurement of eyeball counterroll. *IEEE Transactions on Biomedical Engineering, 2*, 65–70.

Hansard, M., & Horaud, R. (2010). Cyclorotation models for eyes and cameras. *IEEE Transactions on Systems, Man, and Cybernetics, Part B (Cybernetics), 40*(1), 151–161.

Haslwanter, T. (1995). Mathematics of three-dimensional eye rotations. *Vision Research, 35*(12), 1727–1739.

Haslwanter, T., Straumann, D., Hess, B., & Henn, V. (1992). Static roll and pitch in the monkey: Shift and rotation of listing's plane. *Vision Research, 32*(7), 1341–1348.

Hepp, K. (1990). On listing's law. *Communications in Mathematical Physics, 132*(1), 285–292.

Hepp, K. (1995). Theoretical explanations of listing's law and their implication for binocular vision. *Vision Research, 35*(23), 3237–3241.

Hess, B. J., & Misslisch, H. (2016). Three-dimensional ocular kinematics underlying binocular single vision. *Journal of Neurophysiology, 116*(6), 2841–2856.

Hess, B. J., & Thomassen, J. S. (2014). Kinematics of visually-guided eye movements. *PloS One, 9*(4), e95234.

Hooge, I. T. C., & Van den Berg, A. (2000). Visually evoked cyclovergence and extended listing's law. *Journal of Neurophysiology, 83*(5), 2757–2775.

Kono, R., Clark, R. A., & Demer, J. L. (2002). Active pulleys: Magnetic resonance imaging of rectus muscle paths in tertiary gazes. *Investigative Ophthalmology & Visual Science, 43*(7), 2179–2188.

Krejcova, H., Highstein, S., & Cohen, B. (1971). Labyrinthine and extra-labyrinthine effects on ocular counter-rolling. *Acta oto-laryngologica, 72*(1–6), 165–171.

Ludwig, C. J., & Gilchrist, I. D. (2002). Measuring saccade curvature: A curve-fitting approach. *Behavior Research Methods, Instruments, & Computers, 34*(4), 618–624.

McSorley, E., Haggard, P., & Walker, R. (2004). Distractor modulation of saccade trajectories: Spatial separation and symmetry effects. *Experimental Brain Research, 155*(3), 320–333.

Miller, E. F. (1962). Counterrolling of the human eyes produced by head tilt with respect to gravity. *Acta oto-laryngologica, 54*(1–6), 479–501.

Miller, J. M. (2007). Understanding and misunderstanding extraocular muscle pulleys. *Journal of Vision, 7*(11), 10.

Miller, E. F., & Graybiel, A. (1970). *The effect of gravitoinertial force upon ocular counterrolling.* Tech. rep., DTIC Document.

Minken, A., & Van Gisbergen, J. (1994). A three-dimensional analysis of vergence movements at various levels of elevation. *Experimental Brain Research, 101*(2), 331–345.

Misslisch, H., & Hess, B. J. (2000). Three-dimensional vestibuloocular reflex of the monkey: Optimal retinal image stabilization versus listing's law. *Journal of Neurophysiology, 83*(6), 3264–3276.

Misslisch, H., Tweed, D., Fetter, M., Sievering, D., & Koenig, E. (1994). Rotational kinematics of the human vestibuloocular reflex. III. Listing's law. *Journal of Neurophysiology, 72*(5), 2490–2502.

Misslisch, H., Tweed, D., & Hess, B. (2001). Stereopsis outweighs gravity in the control of the eyes. *The Journal of Neuroscience: the Official Journal of the Society for Neuroscience, 21*(3), RC126.

Mok, D., Ro, A., Cadera, W., Crawford, J., & Vilis, T. (1992). Rotation of listing's plane during vergence. *Vision Research, 32*(11), 2055–2064.

Moore, S. T., Clément, G., Raphan, T., & Cohen, B. (2001). Ocular counterrolling induced by centrifugation during orbital space flight. *Experimental Brain Research, 137*(3–4), 323–335.

Nooij, S. A., Bos, J. E., & Groen, E. L. (2008). Orientation of listing's plane after hypergravity in humans. *Journal of Vestibular Research, 18*(2,3), 97–105.

Novelia, A., & O'Reilly, O. M. (2015a). On geodesics of the rotation group so (3). *Regular and Chaotic Dynamics, 20*(6), 729–738.

Novelia, A., & O'Reilly, O. M. (2015b). On the dynamics of the eye: Geodesics on a configuration manifold, motions of the gaze direction and helmholtz's theorem. *Nonlinear Dynamics, 80*(3), 1303–1327.

Radau, P., Tweed, D., & Vilis, T. (1994). Three-dimensional eye, head, and chest orientations after large gaze shifts and the underlying neural strategies. *Journal of Neurophysiology, 72*(6), 2840–2852.

Raphan, T., & Cohen, B. (2002). The vestibulo-ocular reflex in three dimensions. *Experimental Brain Research, 145*(1), 1–27.

Rizzolatti, G., Riggio, L., Dascola, I., & Umiltá, C. (1987). Reorienting attention across the horizontal and vertical meridians: Evidence in favor of a premotor theory of attention. *Neuropsychologia, 25*(1), 31–40.

Schmitz, G., Bock, O., Grigorova, V., & Ilieva, M. (2010). Adaptation of eye and hand movements to target displacements of different size. *Experimental Brain Research, 203*(2), 479–484.

Schreiber, K., Crawford, J. D., Fetter, M., & Tweed, D. (2001). The motor side of depth vision. *Nature, 410*(6830), 819–822.

Schreiber, K. M., & Schor, C. M. (2007). A virtual ophthalmotrope illustrating oculomotor coordinate systems and retinal projection geometry. *Journal of vision, 7*(10), 4.

Taylor, M. J., Roberts, D. C., & Zee, D. S. (2000). Effect of sustained cyclovergence on eye alignment: Rapid torsional phoria adaptation. *Investigative Ophthalmology & Visual Science, 41*(5), 1076–1083.

Tweed, D. (1997). Visual-motor optimization in binocular control. *Vision Research, 37*(14), 1939–1951.

Tweed, D., Cadera, W., & Vilis, T. (1990). Computing three-dimensional eye position quaternions and eye velocity from search coil signals. *Vision Research, 30*(1), 97–110.

Tweed, D., Fetter, M., Andreadaki, S., Koenig, E., & Dichgans, J. (1992). Three-dimensional properties of human pursuit eye movements. *Vision Research, 32*(7), 1225–1238.

Tweed, D., & Vilis, T. (1990). Geometric relations of eye position and velocity vectors during saccades. *Vision Research, 30*(1), 111–127.

Van der Stigchel, S. (2010). Recent advances in the study of saccade trajectory deviations. *Vision Research, 50*(17), 1619–1627.

Van der Stigchel, S., Meeter, M., & Theeuwes, J. (2007a). The spatial coding of the inhibition evoked by distractors. *Vision Research, 47*(2), 210–218.

Van der Stigchel, S., Meeter, M., & Theeuwes, J. (2007b). Top-down influences make saccades deviate away: The case of endogenous cues. *Acta Psychologica, 125*(3), 279–290.

Van Rijn, L., Van der Steen, J., & Collewijn, H. (1992). Visually induced cycloversion and cyclovergence. *Vision Research, 32*(10), 1875–1883.

Van Run, L., & Van den Berg, A. (1993). Binocular eye orientation during fixations: Listing's law extended to include eye vergence. *Vision Research, 33*(5), 691–708.

von Helmholtz, H., & Southall, J. P. C. (2005). *Treatise on physiological optics, Vol. 3.* Courier Corporation.

Wearne, S., Raphan, T., & Cohen, B. (1999). Effects of tilt of the gravito-inertial acceleration vector on the angular vestibuloocular reflex during centrifugation. *Journal of Neurophysiology, 81*(5), 2175–2190.

Wong, A. M. (2004). Listing's law: Clinical significance and implications for neural control. *Survey of Ophthalmology, 49*(6), 563–575.